Theory of core-collapse supernovae

H.-Th. Janka[1], K. Langanke[2,3], A. Marek[1], G. Martínez-Pinedo[2], B. Müller[1]
[1] Max-Planck Institut für Astrophysik, Garching, Germany
[2]Gesellschaft für Schwerionenforschung, Darmstadt, Germany
[3]Institut für Kernphysik, Technische Universität Darmstadt, Germany

February 5, 2008

Abstract

Advances in our understanding and the modeling of stellar core-collapse and supernova explosions over the past 15 years are reviewed, concentrating on the evolution of hydrodynamical simulations, the description of weak interactions and nuclear equation of state effects, and new insights into the nucleosynthesis occurring in the early phases of the explosion, in particular the neutrino-p process. The latter is enabled by the proton-richness of the early ejecta, which was discovered because of significant progress has been made in the treatment of neutrino transport and weak interactions. This progress has led to a new generation of sophisticated Newtonian and relativistic hydrodynamics simulations in spherical symmetry. Based on these, it is now clear that the prompt bounce-shock mechanism is not the driver of supernova explosions, and that the delayed neutrino-heating mechanism can produce explosions without the aid of multi-dimensional processes only if the progenitor star has an ONeMg core inside a very dilute He-core, i.e., has a mass in the 8–10 $M_\odot$ range. Hydrodynamic instabilities of various kinds have indeed been recognized to occur in the supernova core and to be of potential importance for the explosion. Neutrino-driven explosions, however, have been seen in two-dimensional simulations with sophisticated neutrino transport so far only when the star has a small iron core and low density in the surrounding shells as being found in stars near 10–11 $M_\odot$. The explosion mechanism of more massive progenitors is still a puzzle. It might involve effects of three-dimensional hydrodynamics or might point to the relevance of rapid rotation and magnetohydrodynamics, or to still incompletely explored properties of neutrinos and the high-density equation of state.

Hardly any other astrophysical event is as complex and physically diverse as the death of massive stars in a gravitational collapse and subsequent supernova explosion. All four known forces of nature are involved and play an important role in extreme regimes of conditions. Relativistic plasma dynamics in a strong gravitational field sets the stage, weak interactions govern the energy and lepton number loss of the system via the transport of neutrinos from regions of very high opacities to the free-streaming regime, electromagnetic and strong interactions determine the thermodynamic properties, and nuclear and weak interactions change the composition of the stellar gas. Supernova explosions thus offer a fascinating playground of physics on most different scales of length and time and also provide a testbed for new or exotic phenomena. Naturally, these spectacular astrophysical events have attracted — and have deserved — the interest and attention of researchers with very different backgrounds. To the advantage of the field, also Hans Bethe has preserved for many years his interest in the large diversity of physics problems posed by supernovae.

In this article we will discuss some of the progress that has been made in the simulations of stellar core collapse and supernova explosions on the one hand, and in the description of the microphysics input of such models on the other, since Hans Bethe published his grand review article in 1990 [1]. The field is very broad and has experienced also a great expansion after long-soft gamma-ray bursts have been discovered to be linked to extraordinarily energetic explosions of massive stars. A single article can therefore hardly cover all interesting developments satisfactorily. For recent reviews of the theory and observations of stellar collapse events, focussing on different aspects, see Refs. [2, 3, 4, 5].

We will concentrate here on some selected topics, chosen according to our preference but also by their links to contributions from Hans Bethe and his coworkers. After giving a summary of the physical processes and evolutionary stages that lead from stellar core collapse to supernova explosion, we will briefly review the current status of modeling supernovae and of our present understanding of the explosion mechanism, in particular we will also highlight the open ends of the current research. In the subsequent parts of our article we will then concentrate on nuclear and weak interaction physics that plays an important role for developing better numerical models, and we will report new insights brought by such model improvements about the nucleosynthesis during supernova explosions.

1 The current picture of stellar collapse and explosion

At the end of hydrostatic burning, a massive star consists of concentric shells that are the relics of its previous burning phases (hydrogen, helium, carbon, neon, oxygen, silicon). Iron is the final stage of nuclear fusion in hydrostatic burning, as the synthesis of any heavier element from lighter elements does not release energy; rather, energy must be used up. When the iron core, formed in the center of the massive star, grows by silicon shell burning to a mass around the Chandrasekhar mass limit of about 1.44 solar masses, electron degeneracy pressure cannot longer stabilize the core and it collapses. This starts what is called a core-collapse supernova in course of which the star explodes and parts of the star's heavy-element core and of its outer shells are ejected into the Interstellar Medium.

The onset of the collapse and the infall dynamics are very sensitive to the entropy and to the number of leptons per baryon, Y_e [6]. In turn, these two quantities are mainly determined by weak interaction processes, electron capture and β decay. First, in the early stage of the collapse, Y_e decreases by electron capture on (Fe-peak) nuclei, reactions which are energetically favorable when the electrons have Fermi energies of a few MeV at the densities involved. This reduces the increase of the electron pressure with density, thus accelerating the collapse, and shifts the distribution of nuclei present in the core to more neutron-rich material (Fig. 1, upper left panel). Second, many of the nuclei present can also β decay. While this process is quite unimportant compared to electron capture for initial Y_e values around 0.5, it becomes increasingly competative for neutron-rich nuclei due to an increase in phase space related to larger Q_β values.

Electron capture, β decay, and partial photodisintegration of iron-group nuclei to alpha particles cost the core energy and reduce its electron density. As a consequence, the collapse is accelerated. An important change in the physics of the collapse occurs, as the density reaches $\rho_{\rm trap} \approx 10^{12}\,{\rm g/cm^3}$ (Fig. 1, upper right panel). Then neutrinos are essentially trapped in the core, because their diffusion time (due to coherent conservative scattering on nuclei) becomes larger than the collapse time [1]. After neutrino trapping, the collapse proceeds essentially homologously [7], until nuclear densities ($\rho_0 \approx 10^{14}$ g/cm^3) are reached. Since nuclear matter has a much lower compressibility, the homologous core decelerates and bounces in response to the increased nuclear matter pressure. This drives a shock wave into the outer core, i.e. the region of the iron core which lies outside of the homologous core and in the meantime has continued to fall inwards at supersonic speed.

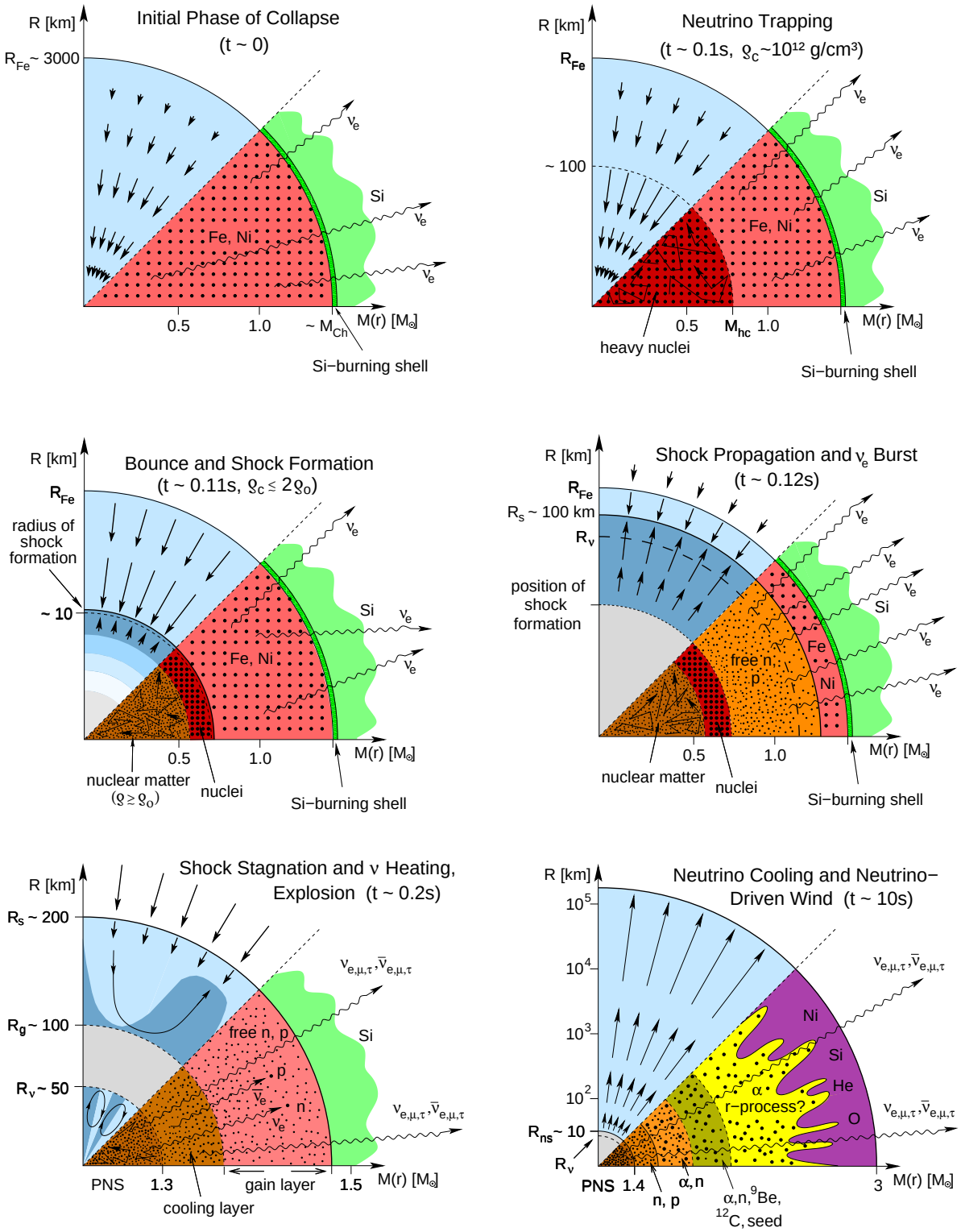

Figure 1: Schematic representation of the evolutionary stages from stellar core collapse through the onset of the supernova explosion to the neutrino-driven wind during the neutrino-cooling phase of the proto-neutron star (PNS). The panels display the dynamical conditions in their upper half, with arrows representing velocity vectors. The nuclear composition as well as the nuclear and weak processes are indicated in the lower half of each panel. The horizontal axis gives mass information. $M_{\rm Ch}$ means the Chandrasekhar mass and $M_{\rm hc}$ the mass of the subsonically collapsing, homologous inner core. The vertical axis shows corresponding radii, with $R_{\rm Fe}$, $R_{\rm s}$, $R_{\rm g}$, $R_{\rm ns}$, and R_ν being the iron core radius, shock radius, gain radius, neutron star radius, and neutrinosphere, respectively. The PNS has maximum densities ρ above the saturation density of nuclear matter (ρ_0).

1.1 Neutrino-driven explosions: spherically symmetric models

The core bounce with the formation of a shock wave is the starting point of a sequence of events that ultimately triggers a supernova explosion (Fig. 1, middle left panel), but the exact mechanism of the explosion and the crucial ingredients of this physically appealing scenario are still uncertain and controversial. If the shock wave is strong enough not only to stop the collapse, but also to explode the outer burning shells of the star, one speaks about the 'prompt mechanism'. However, it appears as if the energy available to the shock is not sufficient, and the shock uses up its energy in the outer core mostly by the dissociation of heavy nuclei into nucleons. This change in composition results in even more energy loss, because the electron capture rate on free protons is significantly larger than on neutron-rich nuclei due to the higher Q-values of the latter. A large fraction of the neutrinos produced by these electron captures behind the shock leave the star quickly in what is called the neutrino burst at shock break-out, carrying away energy. This leads to further neutronization of the matter. The shock is weakened so much that it finally stalls and turns into an accretion shock at a radius between 100 and 200 km, i.e., the matter downstream of the shock has negative velocities and continues falling inward (Fig. 1, middle right panel). All state-of-the-art simulations of stellar core collapse performed in Newtonian gravity [8, 9], with an approximative treatment of general relativity [10, 11, 12], in full general relativity [13, 14, 15, 16, 17], and with stiff or soft nuclear equations of state currently available for core-collapse simulations [18, 19, 20, 21] (see also Sect. 2.1) agree with the models of the 1980's and 1990's (e.g., [22, 23, 24, 25]) that the prompt shock is unable to trigger supernova explosions[1].

After the core bounce, a compact remnant begins to form at the center of the collapsing star, rapidly growing by the accretion of infalling stellar material until the explosion sets in. This nascent remnant — the proto-neutron star — will evolve to a neutron star or may eventually collapse to a black hole, depending on whether the progenitor star had a mass below or above roughly 25 solar masses. The newly born neutron star is initially still proton-rich and contains a large number of degenerate electrons and neutrinos. The latter are trapped because their mean free paths in the dense matter are significantly shorter than the radius of the neutron star. It takes a fraction of a second for the trapped neutrinos to diffuse out [28] (Fig. 1, lower panels). On their way to the neutrinosphere, the neutrinos are down-scattered in energy space, thus converting their initially high degeneracy energy to thermal energy of the stellar medium [29]. The further cooling of the hot interior of the proto-neutron star then proceeds by neutrino-pair production and diffusive loss of neutrinos of all three lepton flavors. After several tens of seconds the compact remnant becomes transparent to neutrinos and the neutrino luminosity drops significantly [30].

In the explosion scenario by the 'delayed neutrino-heating mechanism', the stalled shock wave can be revived by the neutrinos streaming off the neutrinosphere. These neutrinos carry most of the energy set free in the gravitational collapse of the stellar core [28] and deposit some of their energy in the layers between the nascent neutron star and the stalled shock front mainly by charged-current ν_e and $\bar{\nu}_e$ captures on free nucleons [31, 32],

$$\nu_e + n \longrightarrow e^- + p \,, \tag{1}$$

$$\bar{\nu}_e + p \longrightarrow e^+ + n \tag{2}$$

(Fig. 1, lower left panel). This neutrino heating increases the pressure behind the shock and the heated layers begin to expand, creating between shock front and neutron star surface a region of low density but rather high temperature, the so-called 'hot bubble' [33]. The persistent energy input by neutrinos keeps the pressure high in this region and drives the shock outwards again, eventually leading to a supernova explosion. This may take a few 100 ms and requires that during this time interval a few percent of

[1] Successful prompt explosions were found in case of extremely small stellar iron cores [26] or a very soft nuclear equation of state [27], but it is possible that their true reason was the parameterized equation of state or the approximative treatment of neutrino transport used in the simulations.

the radiated neutrino energy (or 10–20% of the energy of electron neutrinos and antineutrinos) are converted to thermal energy of nucleons, leptons, and photons. The canonical explosion energy of a supernova is less than one percent of the total gravitational binding energy lost by the nascent neutron star in neutrinos.

The success of the delayed supernova mechanism turned out to be sensitive to a delicate competition of neutrino cooling between the neutrinosphere and the so-called 'gain radius' on the one hand, and neutrino heating between the gain radius und the shock on the other (Fig. 1, lower left panel). The gain radius is defined as the radial position where the neutrino heating rate per nucleon,

$$Q_\nu^+ \approx 110 \cdot \left(\frac{L_{\nu_e,52} \langle \epsilon^2_{\nu_e,15} \rangle}{r_7^2 \, \langle \mu \rangle_{\nu_e}} \, Y_n \, + \, \frac{L_{\bar\nu_e,52} \langle \epsilon^2_{\bar\nu_e,15} \rangle}{r_7^2 \, \langle \mu \rangle_{\bar\nu_e}} \, Y_p \right) \quad \left[\frac{\mathrm{MeV}}{\mathrm{s} \cdot N} \right] \, , \tag{3}$$

and the neutrino cooling rate per nucleon,

$$Q_\nu^- \approx 145 \left(\frac{k_\mathrm{B} T}{2\,\mathrm{MeV}} \right)^6 \quad \left[\frac{\mathrm{MeV}}{\mathrm{s} \cdot N} \right] \, , \tag{4}$$

become equal. In the latter expression we have used the assumptions that the sum of neutron and proton abundances is unity, $Y_n + Y_p = 1$, and that the electron and positron degeneracy parameters, $\eta_{e^\pm} = \mu_{e^\pm}/(k_\mathrm{B} T)$, are small: $\eta_{e^-} = -\eta_{e^+} \equiv \eta_e \approx 0$. The latter approximation is good in the shock-heated layers because the electron number fraction $Y_e = n_e/n_\mathrm{b}$ (n_e and n_b being the electron and baryon number density, respectively) and thus the electron degeneracy is rather low and $e^\pm$ pairs are abundant. In Eq. (3), r_7 is the radius in 10^7 cm. The neutrino luminosity L_{ν_i} (normalized to $10^{52}\,\mathrm{erg\,s^{-1}}$ in Eq. 3), the average squared neutrino energy $\langle \epsilon^2_{\nu_i} \rangle$ (in units of 15 MeV in Eq. 3), and the mean value of the cosine of the angle between the direction of the neutrino propagation and the radial direction, $\langle \mu_{\nu_i} \rangle$, are calculated from the neutrino phase space occupation function $f_{\nu_i}(\epsilon_\nu, \mu)$ by

$$L_{\nu_i} \;=\; 4\pi r^2 c \, \frac{2\pi}{(hc)^3} \int\limits_0^\infty \mathrm{d}\epsilon_\nu \int\limits_{-1}^{+1} \mathrm{d}\mu \, \mu \, \epsilon_\nu^3 \, f_{\nu_i}(\epsilon_\nu, \mu) \, , \tag{5}$$

$$\langle \epsilon^2_{\nu_i} \rangle \;=\; \int\limits_0^\infty \mathrm{d}\epsilon_\nu \int\limits_{-1}^{+1} \mathrm{d}\mu \, \epsilon_\nu^5 \, f_{\nu_i} \left(\int\limits_0^\infty \mathrm{d}\epsilon_\nu \int\limits_{-1}^{+1} \mathrm{d}\mu \, \epsilon_\nu^3 \, f_{\nu_i} \right)^{-1} , \tag{6}$$

$$\langle \mu_{\nu_i} \rangle \;=\; \int\limits_0^\infty \mathrm{d}\epsilon_\nu \int\limits_{-1}^{+1} \mathrm{d}\mu \, \mu \, \epsilon_\nu^3 \, f_{\nu_i} \left(\int\limits_0^\infty \mathrm{d}\epsilon_\nu \int\limits_{-1}^{+1} \mathrm{d}\mu \, \epsilon_\nu^3 \, f_{\nu_i} \right)^{-1} . \tag{7}$$

The quantity $\langle \mu_\nu \rangle$ is also called flux factor and can be understood as the ratio of the neutrino energy flux, $L_\nu/(4\pi r^2)$, to the neutrino energy density times c. Typically, it is close to 0.25 near the neutrinosphere of ν_e and $\bar\nu_e$ and approaches unity when the neutrino distributions get more and more forward peaked in the limit of free streaming with increasing distance from the neutrinosphere. Angle-dependent transport, i.e., solving the Boltzmann transport equation, is necessary to accurately determine the spectral and angular distribution of the neutrinos.

Only if the heating is sufficiently strong, depending on the size of the neutrino luminosities and the hardness of the neutrino spectra, an explosion can be triggered [32, 34, 35]. The effect is self-enhancing: strong heating of the matter accreted by the shock decelerates the infall and increases the time for matter to absorb neutrino energy, thus raising the efficiency of energy deposition by neutrinos. This positive feedback leads to further shock expansion and can initiate the final runaway. Strong cooling has the opposite effect. It accelerates the accretion flow through the gain layer and largely reduces the time matter is exposed to heating, hence diminishing the chance for an explosion [35]. The Livermore group found the mechanism working successfully only when the neutrino luminosities from the neutron

star were assumed to be boosted by neutron-finger convection below the neutrinosphere (treated by a mixing length theory in the spherically symmetric models) [36, 37]. The existence of neutron-finger instabilities, however, was questioned by independent analysis [38, 39].

In addition to this conflicting situation in a crucial aspect of the successful delayed explosion models, there were long-standing concerns that other approximations or numerical deficiencies of the Livermore models, e.g. in the hydrodynamics scheme or resolution, the flux-limited diffusion description of the neutrino transport, and the treatment of neutrino-matter interactions, might have prevented explosions of the models without the controversial neutron-finger convection. For this reason, improved numerical algorithms for one-dimensional simulations were developed. These are either based on implicit, adaptive-grid solvers for the hydrodynamics and Boltzmann transport equations [40, 16] or use conservative, third-order schemes with a Riemann-solver for the explicit integration of the hydrodynamics equations, coupled to an implicit solver for the moment equations of neutrino number, energy, and momentum with a closure relation (variable Eddington-factor) computed from a model Boltzmann equation [41]. The latter approach is basically Newtonian but employs an effective potential to account for the effects of general relativistic gravity, and includes corrections for gravitational redshift and time dilation in the neutrino transport. Core-collapse calculations with both codes were compared and show very good agreement [17, 42].

Considerable effort has also been spent on implementing weak interaction processes or improvements of the description of such reactions that have been recognized to be of importance in addition to the standard set of processes and their canonical treatment as given by Bruenn [43]. Among these extensions and improvements are shell-model based calculations for β-processes of neutrinos and nuclei (see Sect. 2.2) and for inelastic neutral-current neutrino-nuclei scatterings (see Sect. 2.3), and the inclusion of ion-ion correlations in coherent neutrino-nuclei scatterings [44, 45, 46, 47]. Neutrino interactions with free nucleons have been corrected for nucleon thermal motions and recoil [48] and the weak magnetism [49], and have been generalized for including nucleon correlation effects in high-density media [50, 51, 52, 53]. Of particular importance for the transport of muon and tau neutrinos are nucleon-nucleon bremsstrahlung, $NN \longrightarrow NN\nu\bar{\nu}$ [54, 55], and neutrino-antineutrino annihilation to pairs of other flavors, $\nu_e\bar{\nu}_e \longrightarrow \nu\bar{\nu}$ [56], which dominate e^+e^--annihilation in the production of $\nu_\mu\bar{\nu}_\mu$ and $\nu_\tau\bar{\nu}_\tau$ pairs [57], and to a minor degree also scattering reactions between neutrinos and antineutrinos of different flavors such as $\nu_{\mu,\tau}\nu_e \longrightarrow \nu_{\mu,\tau}\nu_e$ and $\nu_{\mu,\tau}\bar{\nu}_e \longrightarrow \nu_{\mu,\tau}\bar{\nu}_e$. Including all these additional reactions and improvements makes the radiated heavy-lepton neutrino spectra much more similar to the spectra of ν_e and $\bar{\nu}_e$ than previously thought [57]. The similarity of these spectra and the corresponding mean energies at later postbounce times can be clearly seen in Fig. 2.

Spherically symmetric simulations with the new and more accurate hydrodynamics and neutrino transport codes with or without the extended set of neutrino reactions [9, 13, 16, 12, 8, 21], disregarding neutron-finger instabilities and other multi-dimensional effects, agree with the Livermore calculations that no delayed explosions can be obtained for progenitors more massive than $10\,M_\odot$.

In contrast, in case of stars with birth masses of 8–$10\,M_\odot$, which develop instead of an iron core a core of ONeMg with a thin carbon shell, surrounded by an extremely dilute and only loosely bound He-shell, neutrino heating was found to power explosions in one-dimensional (1D) simulations even without convective luminosity enhancement [60]. Also this result of the Livermore group was confirmed qualitatively by more recent models ([58]; Fig. 3), but the more sophisticated neutrino transport in the new simulations produces less energetic explosions of only $1\text{–}2\times10^{50}$ erg (= 0.1–0.2 bethe), in agreement with the estimated kinetic energy of the filaments of the Crab nebula [61]. The latter has been suggested as the remnant of the explosion of a star with ONeMg core because of its small carbon and oxygen abundances and its helium overabundance [62]. Moreover, the early supernova ejecta develop a proton-excess instead of the former neutron-richness (Fig. 3, right panel). This removes the problem of a vast overproduction of some rare, very neutron-rich isotopes in this material (for more discussion of the nucleosynthesis in proton-rich ejecta, see Sect. 3).

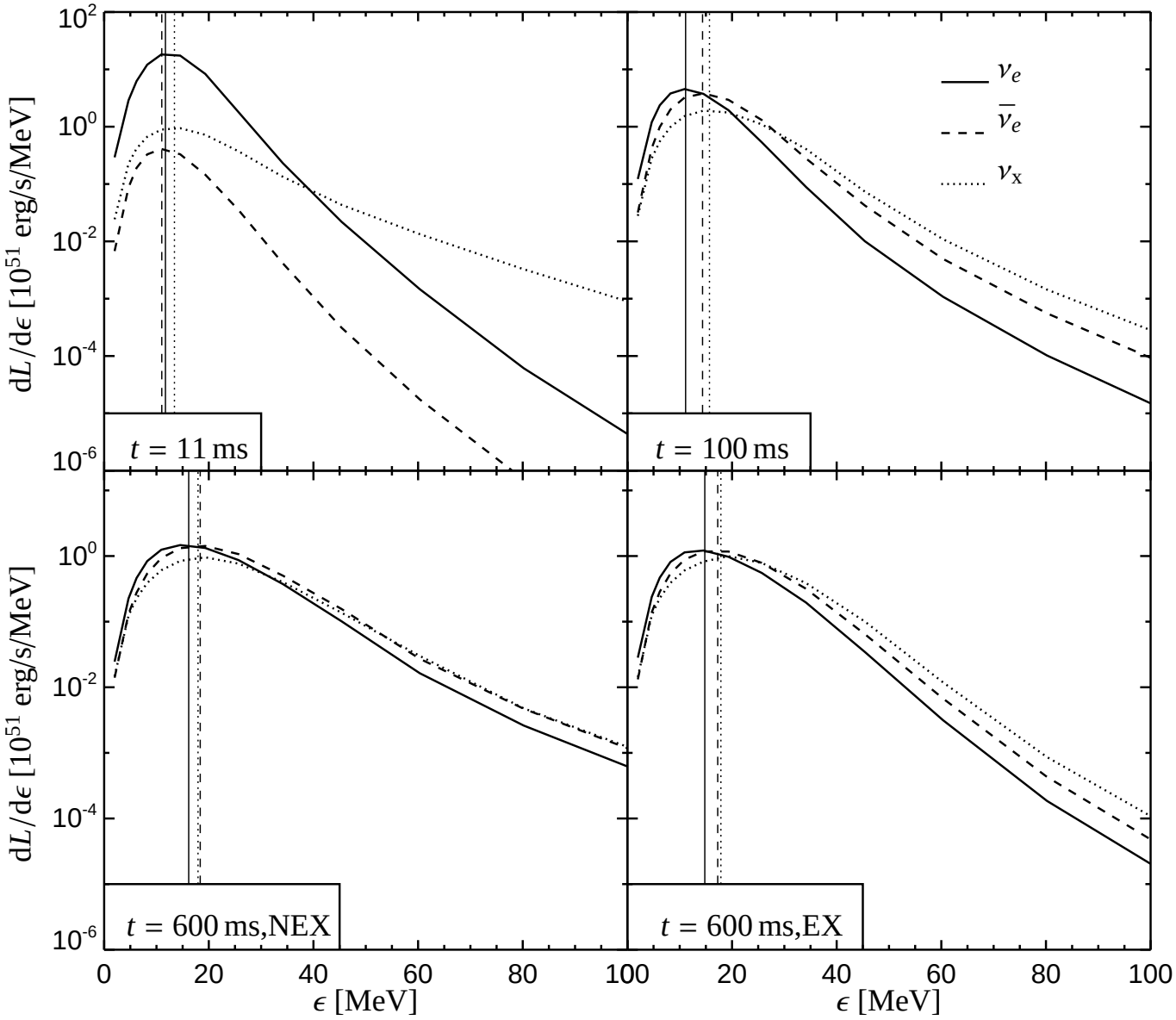

Figure 2: Luminosity spectra for ν_e, $\bar{\nu}_e$, and heavy-lepton neutrinos ν_x for a spherically symmetric $20\,M_\odot$ model. The spectra are given for an observer at rest at 400 km for three different postbounce times: Shortly after the peak of the ν_e shock breakout burst 11 ms after bounce, when the shock is near its maximum radius (around 100 ms p.b.), and at 600 ms after bounce. The lower left panel gives the spectra for a non-exploding model, the lower right panel for a corresponding simulation in which an explosion was artificially initiated at 230 ms after core bounce, thus stopping the accretion onto the nascent neutron star. The vertical lines mark the locations of the mean neutrino energies, which are defined as the ratio of energy flux to number flux, $\langle\epsilon\rangle = L_e/L_n$. Note the similarity of $\langle\epsilon_{\bar{\nu}_e}\rangle$ and $\langle\epsilon_{\nu_x}\rangle$ at $t = 600$ ms (ν_x stands for muon and tau neutrinos and antineutrinos).

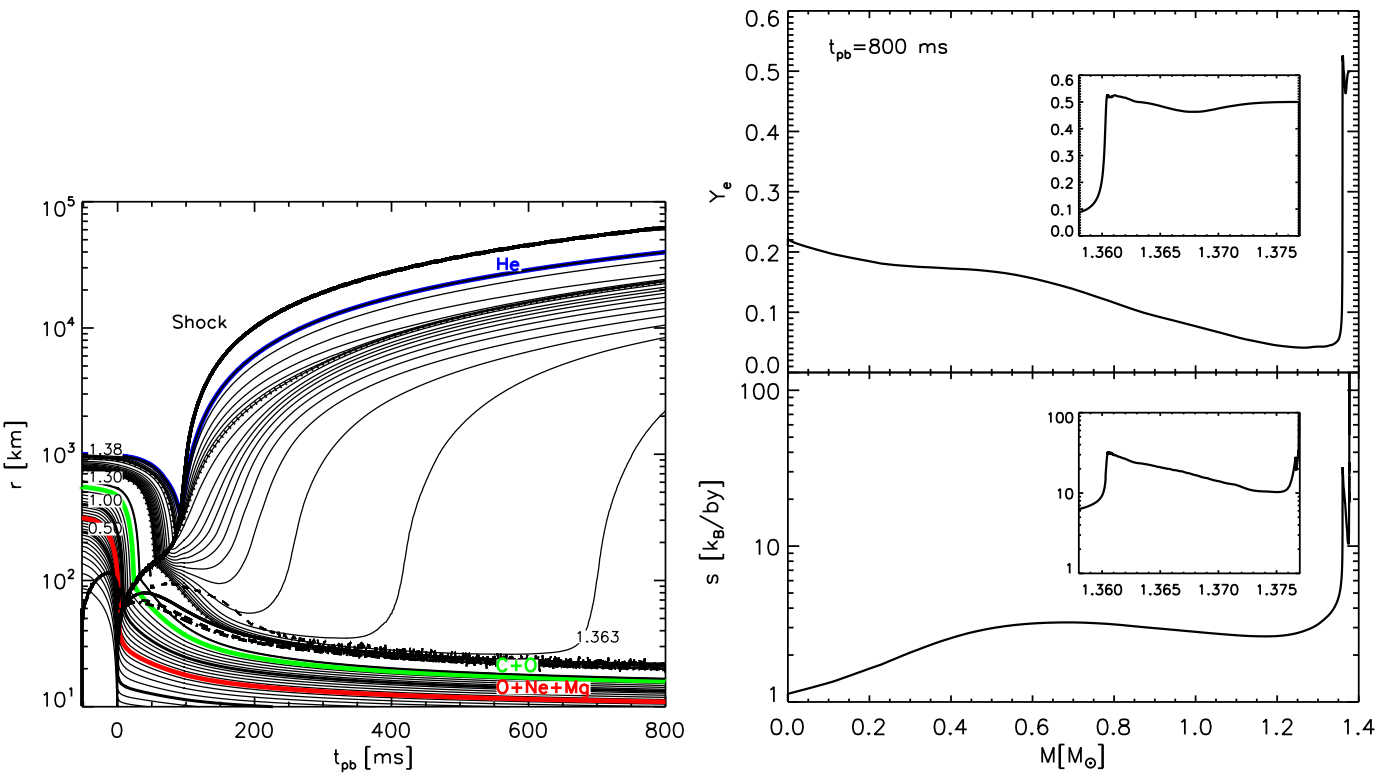

Figure 3: Simulation of collapse and explosion of the ONeMg core of an 8–10 $M_\odot$ star [58, 20]. *Left:* The plot shows the time evolution of the mass shells with the inner boundaries of the O+Ne+Mg shell, C+O shell, and He shell marked by thick (colored) lines. The inner core of about 0.7 $M_\odot$ contains a dominant mass fraction of neon at the onset of collapse [59]. The explosion is driven by the baryonic wind which is caused by neutrino heating around the nascent neutron star. The thick solid, dashed, and dash-dotted lines mark the neutrinospheres of ν_e, $\bar{\nu}_e$, and heavy-lepton neutrinos, respectively, and the thin, dashed line is the gain radius that separates the neutrino-cooling layer below from the neutrino heating layer above. The black thick line starting at $t = 0$ is the outward running supernova shock. Note that the mass shells are chosen with finer spacing at larger radii in the collapsing core. *Right:* Electron fraction Y_e and entropy s versus enclosed mass at the end of the explosion simulation of the ONeMg core. The neutrino-heated ejecta have modest entropies of 10–30 k_B per nucleon and Y_e slightly above or below 0.5. Much less neutron-rich material with less strong neutron excess than in previous models is expelled (figures taken from [58]).

1.2 Neutrino-driven explosions: multi-dimensional models

Hans Bethe in his supernova review of 1990 [1] already pointed out that the hot-bubble region should be convectively unstable (Fig. 1, lower left panel). A negative entropy gradient behind the accretion shock is generated because neutrino heating is much stronger near the gain radius than at larger distances from the neutrinosphere. Multi-dimensional hydrodynamic simulations indeed showed that violent convective overturn develops in this layer and enhances the neutrino-energy deposition there [63, 64, 65, 66, 67, 68]. Neutrino-driven explosions were thus obtained even when spherically symmetric simulations failed [64, 65, 69, 70, 71]. A second convectively unstable region was found to exist inside the newly formed neutron star [72, 73, 74, 12], also indicated in the lower left panel of Fig. 1. It is, however, probably less important for the explosion mechanism because the enhancement of the neutrino emission is rather modest [12].

The success of the first 2D models with postshock convection could not be reproduced by more recent calculations [10, 11, 12, 75, 76] where energy-dependent neutrino transport replaced the simple grey diffusion schemes employed previously. With the currently most sophisticated treatment of neutrino transport that is applied in multi-dimensional supernova simulations (at the same level of refinement in the treatment of neutrino-matter interactions as in the state-of-the-art 1D models), neutrino heating and postshock convection were found to trigger a (probably rather weak) explosion only in case of an $11.2\,M_\odot$ star ([12]; see Fig. 4). The more massive progenitors investigated in Ref. [12] had much higher densities and larger binding energies in the shells surrounding the iron core. The ram pressure associated with the high mass accretion rate of these infalling dense shells damped the shock expansion. Therefore no explosions were obtained for such stars during the simulated evolution periods of about 300 ms after core bounce, although a crucial criterion, the ratio of advection timescale to heating timescale[2], indicates that the critical condition for an explosion was not missed by much (roughly a factor of two in the 2D, 90-degree simulations of Ref. [12]).

The onset of the explosion of the $11.2\,M_\odot$ star was aided by a recently discovered generic instability of the accretion shock to non-radial deformation. This so-called SASI (Standing Accretion Shock Instability; [79]) shows highest growth rates of the $l = 1$, 2 modes (i.e., the dipole and quadrupole terms of an expansion in spherical harmonics) and causes a bipolar sloshing of the shock with pulsational strong expansion and contraction. Since the shock is pushed farther out and the time matter stays in the heating layer therefore increases, this strengthens the neutrino-energy deposition and ultimately leads to a globally asymmetric initiation of the explosion. The rapid growth of this instability can be seeded by the perturbations resulting from the onset of convection in the postshock layer, but occurs also in situations which are convectively stable. It can be understood by an amplifying 'advective-acoustic cycle' in which vorticity perturbations created at the shock are carried inward by the accretion flow, create sound waves when the gas falls onto the neutron star, and the sound waves propagating back to the shock cause larger vorticity perturbations there, closing the feedback loop [80, 81][3]. The SASI was found to be present in all two-dimensional (2D) core-collapse simulations when the calculations were performed with a 180-degree grid and the onset of the explosion was delayed for a sufficiently long time (longer than in the 2D simulations with grey diffusion), thus allowing the instability to develop [83, 84, 12, 75, 76]. The presence of the SASI by itself, however, does not cause the supernova explosion. Different from simulations without neutrinos, where an accumulation of turbulent energy in the postshock layer was found and led to shock expansion [79], this energy accumulation seems to be absent in the neutrino cooled and heated environment of the supernova core. The role of the low-mode

[2]This timescale ratio measures the competing influence of two effects. On the one hand, gas accreted by the stalled shock falls ('is advected') inward on a timescale which measures its exposure to neutrino heating. On the other hand, neutrino heating needs a certain time (the heating timescale) to deposit sufficient energy for matter to become gravitationally unbound [77, 78, 12].

[3]Blondin and Mezzacappa, however, interpret the SASI in their models as a purely acoustic phenomenon in which a standing pressure wave is amplified in the acoustic cavity defined by the shock and the neutrinosphere [2, 82].

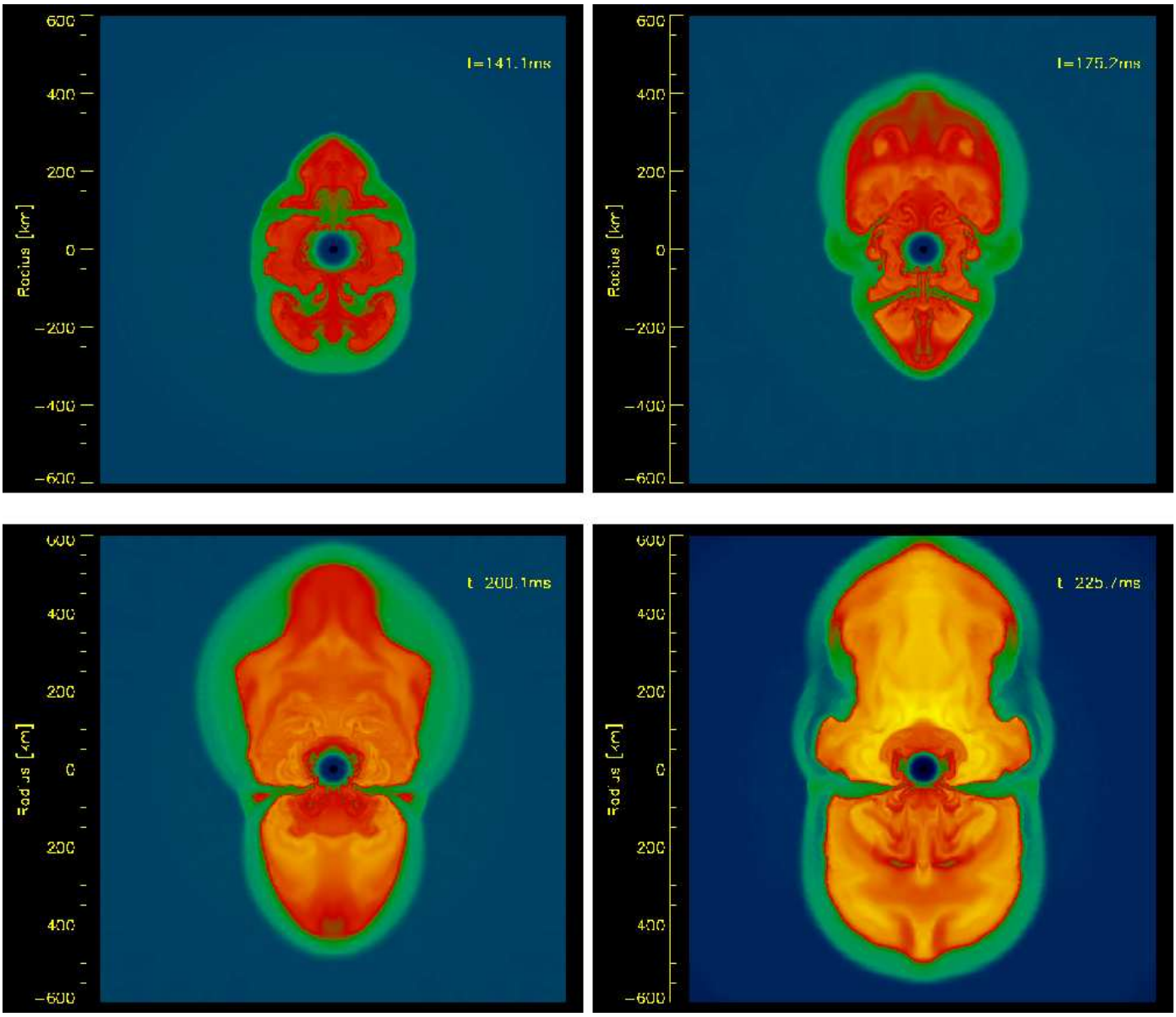

Figure 4: Four stages (at postbounce times of 141.1 ms, 175.2 ms, 200.1 ms, and 225.7 ms) during the evolution of a (non-rotating), exploding two-dimensional $11.2\,M_\odot$ model [12], visualized in terms of the entropy. The scale is in km and the entropies per nucleon vary from about $5\,k_B$ (deep blue), to 10 (green), 15 (red and orange), up to more than $25\,k_B$ (bright yellow). The dense neutron star is visible as low-entropy ($\lesssim 5\,k_B$ per nucleon) circle at the center. The computation was performed in spherical coordinates, assuming axial symmetry, and employing the "ray-by-ray plus" variable Eddington factor technique of Refs. [41, 11] for treating ν transport in multi-dimensional supernova simulations. Equatorial symmetry is broken on large scales soon after bounce, and low-mode hydrodynamic instabilities (convective overturn in combination with the SASI) begin to dominate the flow between the neutron star and the strongly deformed supernova shock. The model develops a — probably rather weak — explosion, the energy of which was not determined before the simulation had to be stopped because of CPU time limitations.

SASI in the successful $11.2\,M_\odot$ model (and also in other simulations) is more indirect. Being stronger than convection, it supports shock expansion and thus significantly improves the conditions for efficient neutrino heating.

The potential importance of this instability for understanding observable properties of supernovae and their remnants was demonstrated recently by a large set of two- and three-dimensional simulations in which neutrino-driven explosions were artificially initiated by chosing a sufficiently high value of the neutrino luminosity of the forming neutron star [83, 84, 85]. These simulations showed that the explosion asymmetry grows stochastically from initial random seed perturbations, breaking the initial sphericity of the collapsing star on a global scale. The highly anisotropic explosions due to a dominant $l = 1$-mode SASI-instability can lead to a large recoil of the newly born neutron star in the direction opposite to the stronger mass ejection. While about half of the computed models produced small neutron star kicks with velocities of only around $100\,\mathrm{km\,s^{-1}}$ or less, the mean value of the recoil velocity was found to be several hundred kilometers per second and even cases with more than $1000\,\mathrm{km\,s^{-1}}$ were obtained, in agreement with the measured proper motions of young pulsars. Three-dimensional simulations have revealed the possibility of an unstable $l = 1$, $m = 1$ spiral SASI mode that can create a strong rotational flow in the vicinity of the accreting neutron star, thus providing a new mechanism for the generation of neutron star spin [86].

Moreover, the globally asymmetric onset of the explosion with sizable initial shock deformation (axis ratios of more than 2:1 were obtained) triggers strong hydrodynamic instabilities at the composition interfaces of the progenitor when the shock propagates outward to the stellar surface. This leads to large-scale element mixing in the exploding star. Iron-group nuclei, silicon, and oxygen, as well as radioactive isotopes are carried from their production sites near the nascent neutron star into the hydrogen envelope, while hydrogen and helium are mixed deep into the expanding ejecta. Supernova simulations in which the SASI-deformed explosion was continuously followed from its initiation by the neutrino-heating mechanism until several hours later for the first time achieved to explain the anisotropies, element mixing, and high nickel velocities observed in Supernova 1987A without invoking artificial and ad hoc assumptions [87]. A unified picture therefore seems to emerge in which hydrodynamic instabilities in the supernova core during the first seconds of the explosion help starting the explosion, create the seed for the ejecta asymmetries observed later on, and are essential for explaining the measured kick velocities and rotation rates of pulsars.

1.3 Alternative explosion scenarios and open ends

But, of course, these conclusions are based on simulations in which neutrino-driven explosions were obtained by a suitable choice of the neutrino luminosities rather than fully self-consistent modeling. What is the missing ingredient why such self-consistent models for progenitor masses larger than about $12\,M_\odot$ have not produced explosions? The situation is currently not clear. Three-dimensional simulations with sophisticated energy-dependent neutrino transport have not been performed yet but are definitely indispensable to judge about the viability of the neutrino-heating mechanism in the more massive progenitor stars, in particular because the critical timescale ratio suggests that the 2D models do not fail by much. In three dimensions the flow dynamics might reveal important differences compared to axisymmetric models, in particular with respect to the growth of convective and Rayleigh-Taylor instabilities, the possibility of non-radial, non-axisymmetric instability modes, or the development of local fluid vortices. Three-dimensional simulations with energy-dependent neutrino transport, however, have such high CPU-time demands that supercomputers ten to hundred times more powerful than currently available will be needed, and numerical codes are necessary that are able to efficiently use thousands of processors. Moreover, although current 2D models do not show a large luminosity boost by neutron star convection [12, 74], the question whether convective or mixing processes below and around the neutrinosphere could more strongly enhance the neutrinospheric neutrino emission and thus

significantly strengthen the neutrino heating behind the shock, must still be considered as unsettled: Doubly diffusive instabilities [39], neutrino-bubble instabilities [88], or magnetic buoyancy instabilities [89] deserve further investigation by multi-dimensional modelling.

Or do explosions require a different mechanism to be at work, for example invoking very rapid rotation of the collapsing stellar core and the amplification of magnetic fields through compression and wrapping, α-Ω dynamo action, or the magneto-rotational instability in the shear flow at the periphery of a differentially rotating nascent neutron star (for a review, see [3])? The fields could then convert the free energy of the differential rotation of the forming compact remnant to kinetic energy of the supernova ejecta either by magnetic forces (e.g., [90, 91, 92, 93, 94] and references therein) or viscous heating behind the shock in addition to the energy input there by neutrinos [78]. Such scenarios, however, seem currently disfavored for ordinary supernovae because of the slow rotation of their progenitors predicted by stellar evolution calculations [95]. Instead, magnetohydrodynamic effects are likely to be the mechanism by which accretion energy is converted to the extreme energy output of hypernovae and the jetted outflow in gamma-ray bursts.

Recently Burrows *et al.*, based on results from their 2D core-collapse simulations, proposed a new acoustic mechanism for launching and powering the explosion [75, 76]. Due to anisotropic accretion, the neutron star in their models is exited to strong g-mode oscillations. The large-amplitude core motions then create powerful sonic activity in the neutron star surroundings by which energy is transported to the shock, driving the explosion. The source of this energy is the gravitational binding energy of the accreted gas, converted to sound by the rapidly ringing neutron star, which thus acts like a transducer. Burrows *et al.* attribute their discovery to the use of a new — according to their arguments superior because linear momentum conserving — treatment of the effects of gravity in their code and the use of a computational grid without the coordinate singularity that is present at the stellar center in the commonly used polar grids. They speculate that the combination of both aspects allows them to see the excitation of the $l = 1$ g-mode oscillations in their 2D simulations, while other groups for numerical reasons can not. This reasoning, however, is questioned by the fact that the 2D models of the Garching group show the presence of this mode and of the higher ($l = 2$, 3, ...) modes in the neutron star as well, all of them with similar, but a factor 10–100 smaller, amplitudes than in the calculations of Burrows *et al.* Moreover, experiments with the code setup used for supernova simulations by the Garching group reveal that a large-amplitude core g-mode, when artificially instigated, can very well be followed over many periods. So the question arises, whether a large-amplitude oscillation as seen by Burrows *et al.* is really excited in the supernova core. And, in particular, will it also be excited when simulations are performed in three dimensions, i.e., without the enforced axial symmetry and associated preferred axis-direction of 2D simulations? Moreover, the core g-mode in the calculations by Burrows *et al.* gains sufficient strength for powering the explosion only at very late postbounce times ($t > 1\,$s; [76]). Neutron stars with large masses are the consequence, and the acoustic mechanism will have its chance only if no other mechanism achieves to explode the star faster (as neutrino heating does, e.g., in case of the exploding 8–11 $M_\odot$ models of Figs. 3 and 4). And even then, the core oscillation energy that is potentially available for the explosion might be rather low, possibly too low to account for explosion energies in agreement with supernova observations.

Significant improvements of all numerical codes currently in use and again 3D simulations will be needed to finally confirm or reject the exitation of strong g-mode $l = 1$ oscillations in the neutron star. Also further improvements of the neutrino transport methods will have to be implemented in the long run [96, 97, 98, 99], because the best energy-dependent schemes that have been applied in full-scale supernova simulations so far either do not couple the energy bins [75, 76] or use approximations to the neutrino transport in non-radial directions [10, 11, 12].

Only recently, collective $\nu\bar{\nu}$-flavor conversion was discovered to be of potential relevance between neutrinosphere and supernova shock [100, 101]. Different from matter-enhanced Mikheyev-Smirnov-Wolfenstein (MSW) neutrino oscillations, which are suppressed in the dense medium of the supernova

core unless the neutrino mass difference is in the eV to keV range — which requires the uncertain existence of a sterile neutrino —, the new flavor transformation process depends only on the presence of a dense neutrino radiation field. Its implications for the supernova explosion mechanism and nucleosynthesis, however, are still unclear and subject of ongoing research.

Finally, but certainly of crucial importance, all further steps of improving supernova simulations must be accompanied and supported by the improvement of the microphysics that plays a decisive role in the supernova core. Electron captures on nuclei, for example, govern the reduction of Y_e during the core collapse phase and thus decide about the shock formation radius and subsequent shock expansion. Similarly, the nuclear equation of state, which is still incompletely known, also influences strongly the shock formation and initial shock strength by its incompressibility at core bounce. The nuclear EoS, moreover, determines the compactness and thus the size and contraction of the nascent neutron star, which in turn influence the shock evolution after bounce. In the following, we will therefore discuss in more detail the nuclear physics input needed for supernova models.

2 Nuclear physics input

2.1 Composition of matter and equation of state

On general grounds the structure of nuclear matter is determined by a competition between the short-ranged surface force and the long-range Coulomb force. The surface energy is reduced with aggregation as this decreases the ratio of surface area to volume. On the other hand, the Coulomb energy is reduced by dispersion as this decreases the inter-proton repulsion. As a result, for densities smaller than about $\rho_0/10$, nucleonic matter consists of individual nuclei, where $\rho_0 = 2.5 \times 10^{14}$ g/cm^3 is the uniform nuclear matter saturation density. However, at larger densities the equilibrium configuration of nuclear matter is achieved by diverse geometrical forms in a competition of uniform nuclear matter and the vacuum [102].

During most of stellar evolution the nuclear composition is determined by a network of nuclear reactions between the nuclei present in the stellar environment. Electromagnetic reactions of the type (p,γ), (α,γ), and once free neutrons are produced, also (n,γ), play a particularly important role to fuse nuclides to successively larger nuclei. As the stellar environment has a finite temperature T, these reactions are in competition with the inverse dissociation reactions ((γ,p), (γ,α), (γ,n)) and for temperatures exceeding $T \approx Q/30$, where Q is the threshold energy (Q-value) for the dissociation process to occur, a capture reaction and its inverse get into equilibrium. Similarly also nuclear reactions mediated by the strong and electromagnetic interaction get into equilibrium with their inverse once the temperature is high enough for the charged particles to effectively penetrate the Coulomb barrier. For supernovae this has the important consequence that for temperatures exceeding a few 100 keVs, all reactions mediated by the electromagnetic and strong interaction are in equilibrium with their inverse and the nuclear composition becomes independent of the rates for these reactions. It is given by Nuclear Statistical Equilibrium (NSE) with the constraints that the total mass and charge of the composition is conserved. The latter condition reflects the fact that charge can only be changed by reactions via the weak interaction which, however, are not in equilibrium as neutrinos can leave the star (until neutrino trapping is effectively reached). Due to the two conserved quantities (mass, charge neutrality) there exist two independent chemical potentials which are conventionally chosen as μ_n and μ_p for neutrons and protons, respectively. In NSE the chemical potential for a nucleus with charge number Z and mass number A is then given by

$$\mu(Z,A) = Z\mu_p + (A-Z)\mu_N. \tag{8}$$

The nuclei obey Boltzmann statistics. Thus the number density $n(Z,A)$ of a nucleus (mass $m(Z,A)$) is related to its chemical potential via

$$\mu(Z,A) = m(Z,A)c^2 + kT \ln\left[\frac{n(Z,A)}{G(Z,A)}\left(\frac{2\pi\hbar^2}{m(Z,A)kT}\right)^{3/2}\right] \tag{9}$$

with the nuclear partition function

$$G(Z,A) = \sum_i (2J_i+1)e^{-E_i/kT}, \tag{10}$$

where the sum runs over all nuclear states with excitation energy E_i and total angular momentum J_i. Upon inserting (9) into (8), one obtains the Saha equation which relates the abundance ($Y(Z,A)\rho/m_u = n(Z,A)$) of a nucleus to the proton and neutron abundances

$$Y(Z,A) = \frac{G(Z,A)A^{3/2}}{2^A}(\rho N_A)^{A-1}Y_p^Z Y_n^N \left(\frac{2\pi\hbar^2}{m_u kT}\right)^{3/2(A-1)} e^{E_b(Z,A)/kT} \tag{11}$$

with $E_b(Z,A) = (Nm_n + Zm_p - M(Z,A))c^2$ and the constraints $\sum_i Y_i A_i = 1$ (conservation number nucleons) and $\sum_i Y_i Z_i = Y_e$ (charge neutrality), where the sum runs over all nuclei present in the composition and Y_e is the electron-to-nucleon ratio. Due to charge neutrality, this is identical to the proton-to-nucleon ratio.

The fact that temperatures are high enough in the late stage of stellar evolution to drive matter into NSE facilitates simulations significantly as the matter composition becomes independent of the rates for reactions mediated by the electromagnetic and strong interaction. In practice, stellar evolution is studied in two steps: The star is followed through its various hydrostatic core and shell burning stages considering an appropriate nuclear network and taking advantage of the fact that neutrinos can leave the star unhindered and thus serve only as a source for energy losses. The simulations stop once the star reaches the *presupernova* stage; i.e. the inner stellar core collapses with velocities in excess of 1000 km/s, which is achieved when the central density and temperatures are of order $10^{10}\,\mathrm{g/cm^3}$ and $10^{10}\,\mathrm{K}$ (860 keV) [103, 104]. The presupernova models (which assume spherical symmetry) become the input of the actual supernova simulations, which explicitly assume that NSE is established. Nevertheless the nuclear composition changes quite drastically during the collapse as temperature and density increase as the collapse progresses and, importantly, the weak interaction is initially not in equilibrium. As we will discuss in the next section, electron captures on nuclei and on free protons occur which reduce Y_e and the nuclear composition is shifted to nuclei with larger neutron excess (smaller proton-to-nucleon ratio) which favors heavier nuclei. The increasing temperature has the consequence that the number of nuclei present in the composition with sizable abundances grows. This effect and the shift to heavier and more neutron-rich nuclei is confirmed in Fig. 5 which shows the NSE abundance distribution for two typical conditions during the collapse. Note that with increasing density, correlations among the nuclei and effects of the surrounding plasma become increasingly relevant [105, 106, 107].

At densities larger than about $\rho_0/10$, the matter composition experiences a drastic change resulting in a variety of complex shapes. This complexity arises as the nucleons try to be simultaneously correlated due to the nuclear attraction and anti-correlated due to Coulomb repulsion. Furthermore, surface tension favors spherical shapes, while the Coulomb interaction often favors other geometrical shapes. As a consequence the transition from individual nuclei to uniform nuclear matter occurs in various steps: from large spherical nuclei immersed into the vacuum, to rod-like geometry, to slabs of uniform matter, to cylindrical bubbles (tubes), to spherical bubbles of vacuum immersed in uniform matter and finally to uniform nuclear matter [108, 109]. Reminded by the shapes of the various transitions at subnuclear densities one often speaks of *nuclear pasta*. More recent studies of the ground state properties of nuclear pasta can be found in [110]; attempts of investigating the dynamical properties of nuclear pasta are reported for example in [111, 112, 113].

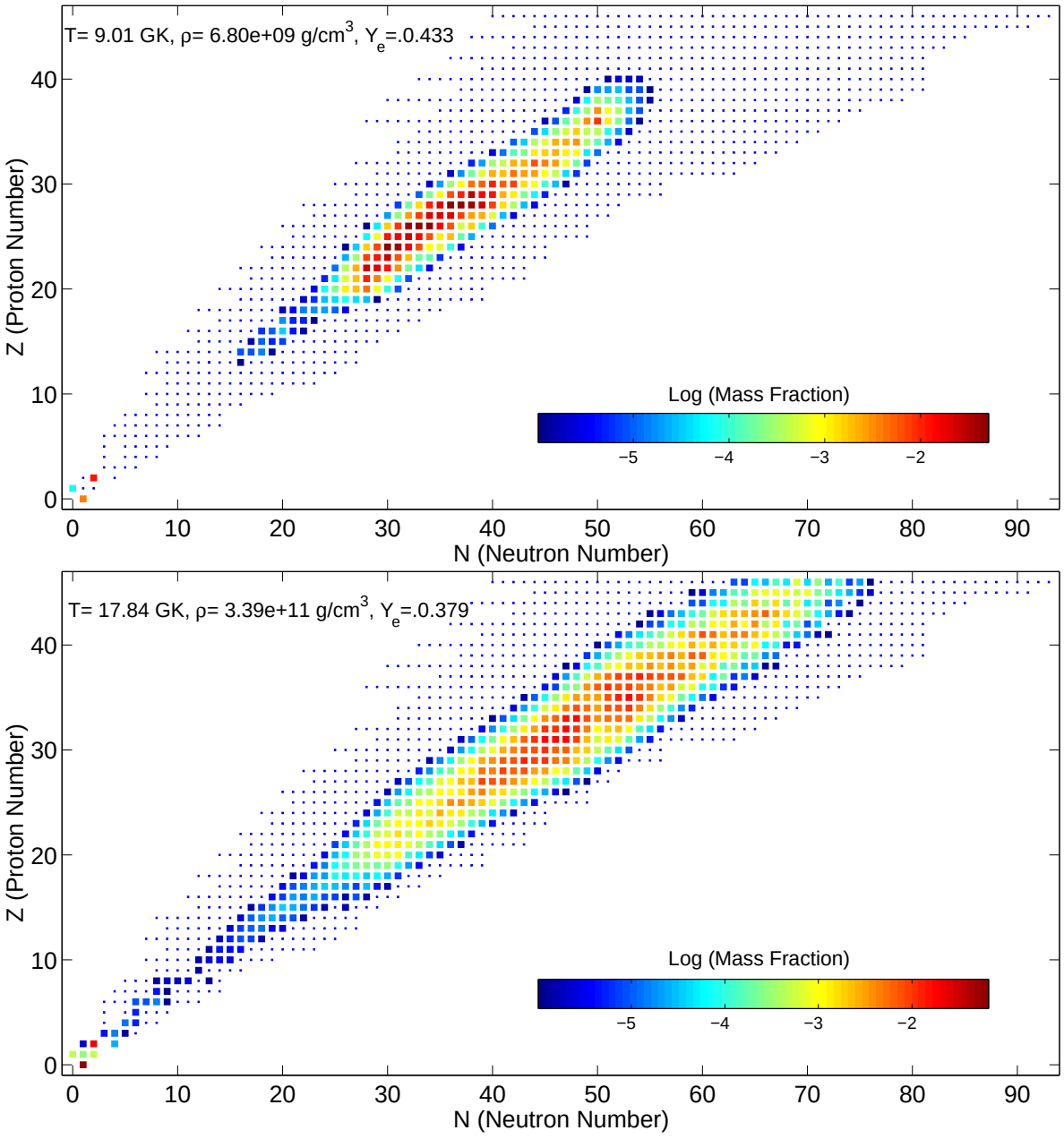

Figure 5: Abundance distributions of nuclei in Nuclear Statistical Equilibrium at conditions which resemble the presupernova stage (top) and the neutrino trapping phase (bottom) of core-collapse simulations (courtesy of W.R. Hix).

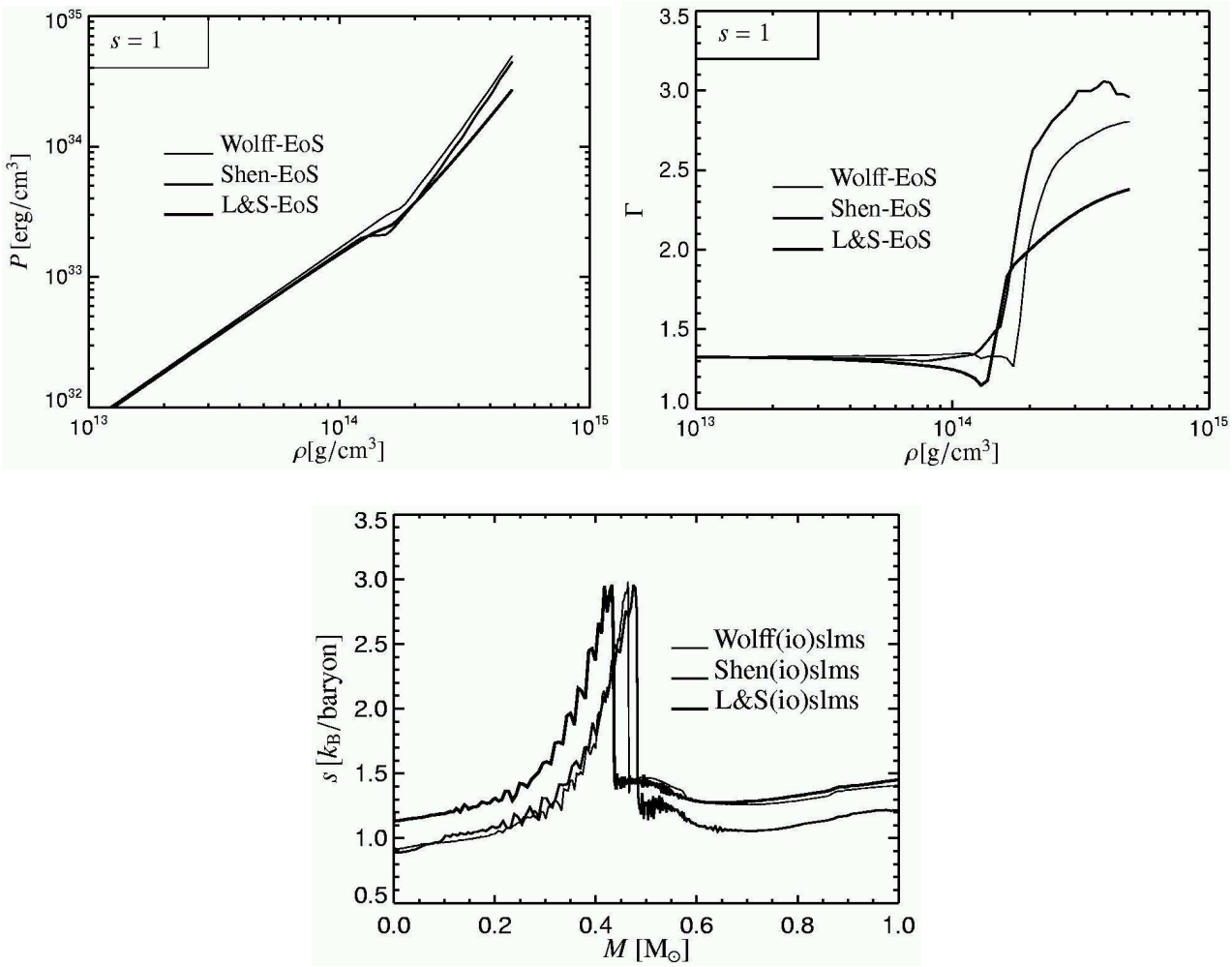

Figure 6: Pressure and adiabatic index $\Gamma \equiv (\partial \ln P/\partial \ln \rho)_s$ vs. mass density for an entropy $s = 1\,k_\mathrm{B}$ per nucleon and $Y_e = 0.4$, and entropy profile vs. enclosed mass at the time of shock formation for simulations with the EoSs of Wolff & Hillebrandt ("Wolff", thin lines; [115]), Shen et al. ("Shen", medium; [116]), and Lattimer & Swesty ("L&S", thick; [117]).

In the shock-heated region temperature gets so high that nuclear matter is dissolved in free protons and neutrons.

The transition region of shape complexity requires also special care in the derivation of the equation of state (EoS) which describes the relevant thermodynamical quantities as function of 3 independent input parameters, e.g. density, temperature and electron-to-nucleon ratio. In the range of temperature and densities relevant for supernovae modelling matter can be modelled as a mixture of electrons, positrons, photons and nuclear constituents. The description is simplified by the justified assumption that matter is in equilibrium with respect to electromagnetic and strong interactions (this assumption is not being made in presupernova simulations). Although nuclear matter composition is then described by a Saha equation, an explicite consideration of all possible nuclei (and nuclear shapes) is computationally yet unfeasible. Thus nuclear matter is represented by four species: free protons, free neutrons, alpha-particles (which represent all light particles present) and an individual heavy nucleus standing in as a representative for the ensemble of heavy nuclei present. With changing inputs (ρ, T, and Y_e) the mass and charge number of this average nucleus is readjusted. Burrows and Lattimer have shown that such a single-nucleus average for the true ensemble of heavy nuclei has little effect on the thermodynamical properties [114]. However, it is not justified in the calculation of the weak interaction rates, as we will discuss in the next section.

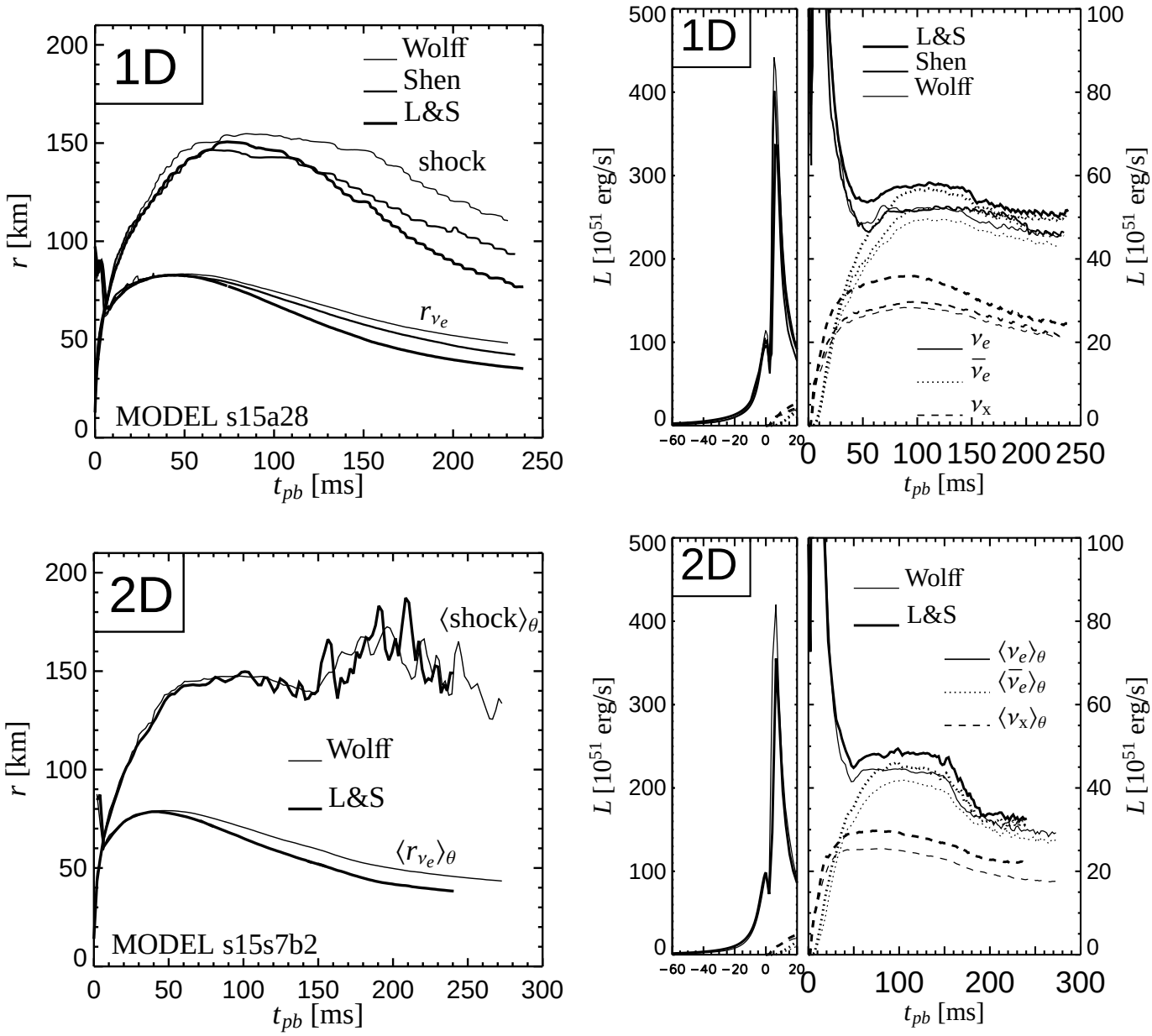

Figure 7: *Top:* Results from 1D core-collapse simulations with the equations of states (EoSs) "Wolff", "Shen", and "L&S" (cf. Fig. 6) for the $15\,M_\odot$ progenitor model s15a28 from Heger et al. [104]. *Bottom:* Results from 2D core-collapse simulations with the equations of states "Wolff" and "L&S" for the $15\,M_\odot$ progenitor model s15s7b2 from Woosley & Weaver [103], using the Garching "ray-by-ray plus" variable Eddington factor technique of Refs. [41, 11] for treating ν transport in multi-dimensional models. The left panels show the shock positions and neutrinosphere radii of ν_e as functions of postbounce time, the right panels display the neutrino luminosities with the prompt ν_e burst in the left window and the postbounce luminosities of ν_e (solid lines), $\bar{\nu}_e$ (dotted) and heavy-lepton ν's and $\bar{\nu}$'s (dashed) in the right window. The results of the 2D runs were averaged over latitudinal angles θ. The left plots demonstrate that the different neutron star contraction for the three equations of state forces the stalled shock to retreat significantly differently during the postbounce evolution in 1D models, whereas the postshock convection in the 2D simulations covers the EoS influence completely despite the remaining (but somewhat reduced) differences of the neutron star radii as functions of time. Because of the latter fact the neutrino luminosities reveal significant differences both in the 1D and 2D cases, because the softer nuclear phase in particular of the L&S EoS leads to higher neutrinospheric temperatures. Note that a detailed comparison of the upper and lower plots is hampered by the use of different $15\,M_\odot$ progenitors.

For more than a decade, the standard EoS in supernova simulations has been the one of Lattimer and Swesty [117]. These authors derive the EoS by minimization of the free energy of the matter. The nuclear part is derived in the spirit of the finite-temperature compressible liquid-drop model [117] treating nuclei within the Wigner-Seitz approximation, e.g. a heavy nucleus in a unit cell is surrounded by a charge-neutral spherical cell made of a gas of neutrons, protons and alpha-particles. Possible effects of neutron skins are ignored. To describe the shape phase transition regime between $\rho_0/10$ and ρ_0, a shape function is introduced which correctly reproduces the limiting cases of nuclei (low density) and bubbles (high density) and in-between approximates more elaborate calculations performed by Ravenhall *et al.* at zero temperatures [108]. The parameters required in the functional form of the free energy were adjusted either to experiment or to some standard Skyrme interaction. The electrons are modelled as non-interacting ultrarelativistic particles, photons are treated as ideal Bose gas. For most of the supernova density-temperature regime, the EoS is dominated by electrons, photons or bulk nuclear matter. As stated above, the largest impact of the nuclear constituents are found in the shape transition region, which likely is also the region of largest uncertainty in the EoS. For supernova simulations density regions larger than twice saturation density are of less interest. Thus, the Lattimer-Swesty EoS does not attempt to describe potential phase transitions to pion or kaon condensates or quark-hadron phases of matter and also does not include the effects of hyperons (e.g. [118]).

The Lattimer-Swesty EoS has recently been improved and is now applicable for temperatures $T = 1 - 30$ MeV and densities between 10^7 g/cm^3 and $6\rho_0$. The improved EoS now explicitly accounts for neutron skin effects and is built on both non-relativistic potential models and relativistic field models.

An alternative EoS has been presented by Shen *al.* [116], based on the Thomas-Fermi spherical cell model and deriving the matter energy from relativistic field theoretical (Brueckner-Hartree-Fock) models. However, this EoS does not consider non-spherical geometries and consequently the shape transition region at sub-saturation densities is approximated by a sudden switch from a nuclear composition to uniform nuclear matter.

The Garching group has used both the Lattimer-Swesty EoS (chosing a soft version with an incompressibility modulus of bulk nuclear matter of 180 MeV and a symmetry energy of 29.3 MeV) and the harder Shen-EoS (with an incompressibility of 281 MeV and a symmetry energy of 36.9 MeV) in 1D as well as 2D supernova simulations, and compared the results with models in which the EoS of Hillebrandt and Wolff [115] was employed [18, 20, 121, 122]. The latter was constructed by a temperature-dependent Hartree-Fock calculation with a Skyrme force for the nucleon-nucleon interaction. It has an incompressibility parameter of 263 MeV and a symmetry energy of 32.9 MeV. The three equations of state show clear differences for example in the nuclear composition during the core-collapse phase and in the adiabatic index $\Gamma \equiv (\partial \ln P/\partial \ln \rho)_s$ around and above the phase transition to homogeneous nuclear matter (Fig. 6). Due to a much larger abundance of free protons and a longer collapse time, the L&S EoS leads to a considerably stronger deleptonization in the infall phase and therefore a shock-formation position that is significantly inside the one obtained with the Shen EoS (Fig. 6, right panel). In none of the 1D simulations for different progenitors with $M > M_\odot$ an explosion was obtained. Since the radius of the stalled shock follows closely the initial growth of the radius of the nascent neutron star due to mass accretion and the following shrinking of the settling neutron star, the radii of maximum shock expansion and subsequent shock contraction also differ in 1D simulations with the three EoSs (Fig. 7, upper left panel). A more compact and thus hotter neutron star also leads to higher neutrino luminosities and larger mean energies of the neutrinos radiated during the postbounce evolution (Fig. 7, right panels). Similar findings, although quantitatively somewhat different — probably because of numerical reasons — were obtained by Sumiyoshi et al. [21], who also continued their simulations for the L&S and Shen-EoSs to a postbounce time as late as 1 s.

2.2 Neutrino-nuclei beta-interactions

Nuclear processes, mediated by the weak-interaction, play an essential role during the collapse. While positron captures on nuclei and nuclear β^+ decays are also considered in supernova simulations, the two important weak processes are nuclear beta-decay

$$(Z, A) \rightarrow (Z + 1, A) + e^- + \bar{\nu_e} \tag{12}$$

and electron capture

$$(Z, A) + e^- \rightarrow (Z - 1, A) + \nu_e. \tag{13}$$

Both processes have in common that they create neutrinos and that they change the number of electrons. Both of these properties are quite important: the neutrinos leave the star nearly unhindered for core densities smaller than a few 10^{11} g/cm^3 and carry away energy in this way cooling the stellar core and keeping its entropy low [6]. As electrons dominate the matter pressure during most of the collapse (for densities less than 10^{13} g/cm^3), a change of the electron number density (or better in the electron-to-baryon ratio Y_e) directly influences the collapse dynamics.

Except at rather high densities, nuclear beta-decays and electron captures are dominated by allowed transitions. For beta-decays (and nuclei with neutron excess), these are Fermi transitions (which for each parent state can only proceed to a single state in the daughter nucleus, the isobaric analog state) and Gamow-Teller transitions GT$_-$, in which a neutron is changed into a proton. Under core-collapse conditions electron captures are dominated by Gamow-Teller (GT) transitions GT$_+$, in which a proton is changed into a neutron. Gamow-Teller transitions are mediated by the operator $\sigma\tau_\pm$ where σ is the spin operator and $\tau_\pm$ are the isospin raising or lowering operators, respectively.

As the stellar interior has finite temperature T, beta decays and electron captures can occur from excited nuclear levels, where the thermal nuclear ensemble is described by a Boltzmann distribution. Beta-decay λ_β and electron capture rates λ_{ec} can be derived in perturbation theory and the respective formulas and derivations are presented in [119, 120]. One obtains

$$\lambda_\beta = \frac{\ln 2}{K} \sum_i \frac{(2J_i + 1)e^{-E_i/(kT)}}{G(Z, A, T)} \sum_j (B_{ij}(F) + B_{ij}(GT))\Phi_{ij}^\alpha, \tag{14}$$

$$\lambda_{ec} = \frac{\ln 2}{K} \sum_i \frac{(2J_i + 1)e^{-E_i/(kT)}}{G(Z, A, T)} \sum_j B_{ij}(GT)\Phi_{ij}^\alpha, \tag{15}$$

where K can be determined from superallowed Fermi transitions, $K = 6146 \pm 6$ s [123]. $G(Z, A, T) = \sum_i (2J_i + 1) \exp(-E_i/(kT))$ is the partition function of the parent nucleus. B_{ij} is the reduced transition probability of the nuclear transition, where we have restricted ourselves to allowed transitions only.

The Fermi transition strength is given by:

$$B_{ij}(F) = \frac{\langle j || \sum_k \mathbf{t}_\pm^\mathbf{k} || \mathbf{i} \rangle^\mathbf{2}}{2J_i + 1}. \tag{16}$$

If isospin is a good quantum number, the Fermi transition strength is concentrated in the isobaric analog state (IAS) of the parent state. Equation (16) reduces to,

$$B_{ij}(F) = T(T + 1) - T_{z_i} T_{z_j}, \tag{17}$$

where j denotes the IAS of the state i. Here the reduction in the overlap between nuclear wave functions due to isospin mixing has been neglected as it is estimated to be small ($\approx 0.5\%$ [123]).

The GT strength is given by:

$$B_{ij}(GT) = \left(\frac{g_A}{g_V}\right)^2_{\rm eff} \frac{\langle j||\sum_k \sigma^{\mathbf{k}} \mathbf{t}^{\mathbf{k}}_{\pm}||\mathbf{i}\rangle^{\mathbf{2}}}{2J_i+1}, \tag{18}$$

where the matrix element is reduced with respect to the spin operator σ only (Racah convention [124]) and the sum runs over all nucleons. For the isospin rising and lowering operators, $\mathbf{t}_{\pm} = (\tau_{\mathbf{x}} \pm \mathbf{i}\tau_{\mathbf{y}})/\mathbf{2}$, we use the convention $\mathbf{t}_{+}\mathbf{p} = \mathbf{n}$; thus, '+' refers to electron capture and '−' to β^- transitions. Finally, $(g_A/g_V)_{\rm eff}$ is the effective ratio of axial (g_A) and vector (g_V) coupling constants that takes into account the observed quenching of the GT strength [125]. We use [126]

$$\left(\frac{g_A}{g_V}\right)_{\rm eff} = 0.74 \left(\frac{g_A}{g_V}\right)_{\rm bare}, \tag{19}$$

with $(g_A/g_V)_{\rm bare} = -1.2599(25)$ [123]. If the parent nucleus (with isospin T) has a neutron excess, then the GT_- operator can connect to states with isospin $T-1$, T, $T+1$ in the daughter, while GT_+ can only reach states with $T+1$. This isospin selection is one reason why the GT_+ strength is more concentrated in the daughter nucleus (usually within a few MeV around the centroid of the GT resonance), while the GT_- is spread over 10-15 MeV in the daughter nucleus and is significantly more structured. The difference of the total GT strengths in the β^- and electron capture directions is fixed to the threefold of the neutron excess ($N-Z$) which is known as the Ikeda sumrule [127].

The last factor in equation (14), Φ^{α}_{ij}, is the phase space integral given by

$$\begin{aligned} \Phi^{ec}_{ij} = \int_{w_l}^{\infty} w \quad & p \quad (Q_{ij}+w)^2 F(Z,w) \\ & \times \quad S_e(w)(1-S_\nu(Q_{ij}+w))dw, \end{aligned} \tag{20}$$

$$\begin{aligned} \Phi^{\beta^-}_{ij} = \int_{1}^{Q_{ij}} w \quad & p \quad (Q_{ij}-w)^2 F(Z+1,w) \\ & \times \quad (1-S_e(w))(1-S_\nu(Q_{ij}-w))dw, \end{aligned} \tag{21}$$

where w is the total, rest mass and kinetic, energy of the electron or positron in units of $m_e c^2$, and $p = \sqrt{w^2-1}$ is the momentum in units of $m_e c$. Then the total energy available in β-decay, Q_{ij}, in units of $m_e c^2$ is given by

$$Q_{ij} = \frac{1}{m_e c^2}(M_p - M_d + E_i - E_j), \tag{22}$$

where M_p, M_d are the nuclear masses of the parent and daughter nucleus, respectively, while E_i, E_j are the excitation energies of the initial and final states. w_l is the capture threshold total energy, rest plus kinetic, in units of $m_e c^2$ for positron (or electron) capture. Depending on the value of Q_{ij} in the corresponding electron (or positron) emission one has $w_l = 1$ if $Q_{ij} > -1$, or $w_l = |Q_{ij}|$ if $Q_{ij} < -1$. S_e, S_p, and S_ν are the positron, electron, and neutrino (or antineutrino) distribution functions, respectively. For core-collapse conditions, electrons and positrons are well described by Fermi-Dirac distributions, with temperature T and chemical potential μ. For electrons,

$$S_e = \frac{1}{\exp\left(\frac{E_e-\mu_e}{kT}\right)+1}, \tag{23}$$

with $E_e = w m_e c^2$. The positron distribution is defined similarly with $\mu_p = -\mu_e$. The chemical potential, μ_e, is determined from the density inverting the relation

$$\rho Y_e = \frac{1}{\pi^2 N_A}\left(\frac{m_e c}{\hbar}\right)^3 \int_0^\infty (S_e - S_p) p^2 dp, \tag{24}$$

where N_A is Avogadro's number. Note that the density of electron-positron pairs has been removed in (24) by forming the difference $S_e - S_p$.

The remaining factor appearing in the phase space integrals is the Fermi function, $F(Z, w)$, that corrects the phase space integral for the Coulomb distortion of the electron or positron wave function near the nucleus. It can be approximated by

$$F(Z, w) = 2(1+\gamma)(2pR)^{-2(1-\gamma)} \frac{|\Gamma(\gamma + iy)|^2}{|\Gamma(2\gamma+1)|^2} e^{\pi y}, \tag{25}$$

where $\gamma = \sqrt{1-(\alpha Z)^2}$, $y = \alpha Z w/p$, α is the fine structure constant, and R is the nuclear radius.

Laboratory studies of β-decays and electron captures can only observe the GT strength within the Q_β value, i.e. the part of the GT strength which is energetically reachable. Unfortunately this is usually only a small part of the GT strength distribution. A breakthrough in experimental investigations of GT distributions has been achieved with the study of charge-exchange reactions at intermediate projectile energies where the reaction cross section at extreme forward angles is proportional to the GT strength. Hence, using the pioneering probes like (p,n) and (n,p) reactions it has been possible to measure the GT_- and GT_+ strength distributions, respectively, over a large excitation energy interval [128, 129]. These experiments revealed two quite decisive results: At first, the GT strength is distributed over many states in the daughter nucleus caused by the residual nuclear interaction which does not commute with the $\sigma \mathbf{t}_\pm$ operator. Secondly, the GT strength is 'quenched'. As the GT operator does not act on the spatial nuclear wave functions it cannot connect nuclear orbitals in different harmonic oscillator shells. However, it has been found that so-called $0\hbar\omega$ shell model calculations, which account for all two-nucleon correlations of the valence nucleons within one major oscillator shell, overestimate the measured GT strengths by a constant factor (which lead to the introduction of the effective axial-vector coupling constant as discussed above) [130, 131]. The origin of the quenching is mainly due to higher-shell admixtures in the ground state wave function which causes a portion of the GT strength to be shifted to moderately high excitation energies. In fact, by detailed (p,n) reaction studies on ^{90}Zr GT_- strength has been identified up to excitation energies of order 90 MeV [132].

While the GT data from the (p,n) and (n,p) experiments have been inexpensible for the understanding of GT distributions in nuclei, these probes have relatively poor energy resolution, in particular the (n,p) experiments. Nowadays high-resolution measurements of the GT strengths are possible due to the development of (^{3}He,t) [133] and (d,^{2}He) [134] reaction probes which allow to determine the GT_- and GT_+ strength with a resolutions of 30 keV and 150 keV, respectively. Although experimentally one can only determine the GT strength distributions for nuclear ground states, these data serve as precious constraints and tests for the nuclear models which are then required to evaluate the GT strengths for the excited nuclear states which are needed to calculate the β-decay and electron capture rates at finite temperatures.

Before we discuss which reactions are important and how one can calculate the relevant reaction rates, it is useful to compare the various energy scales of the problem. This is done in Fig. 8 which shows the electron chemical potential μ_e and typical core temperatures and nuclear Q-values (defined as $\mu_n - \mu_p$, the difference of neutron and proton chemical potential) as functions of the central stellar density. Obviously μ_e, which is proportional to $\rho^{1/3}$, grows much faster than the other energies. This has several important quantities:

1. With growing density nuclear beta-decays are increasingly hindered by the presence of electrons which block the available decay phase space. For densities larger than 10^{10} g/cm^3 beta-decays are effectively irrelevant. As we will show below, this is quite fortuitious as reliable beta-decay

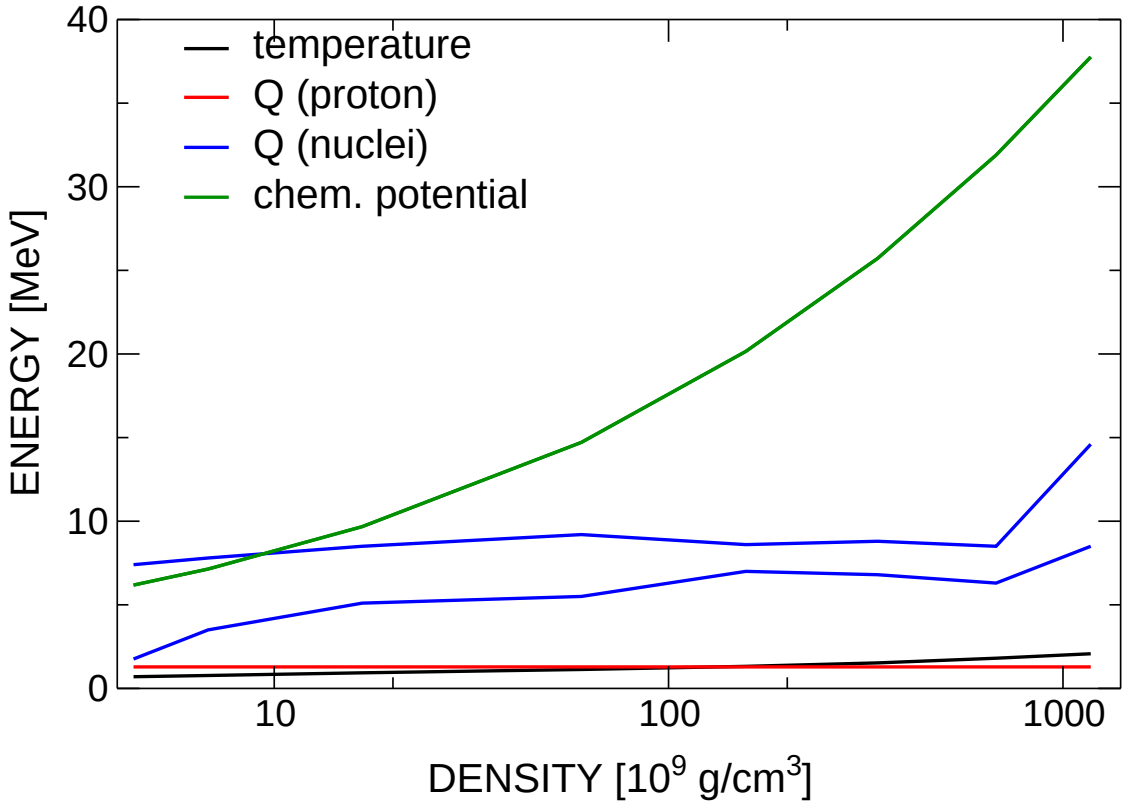

Figure 8: Sketch of the various energy scales related to electron capture on protons and nuclei as a function of densitiy during a supernova core collapse simulation. Shown are the chemical potential, respectively Fermi energy, of electrons, the Q-values for electron capture on free protons (constant), and the average Q-value for electron capture on nuclei for the given composition at each density.

rates are difficult to calculate, but for supernova simulations are only required for nuclei for which large-scale shell model calculations can be performed.

2. For densities ρ less than a few 10^{10} g/cm^3, the electron chemical potential is of the same order of magnitude as the nuclear Q-value. Hence electron capture rates are quite sensitive to the detailed GT$_+$ strength distribution. Fortunately under such conditions electron capture mainly occurs on nuclei in the mass range $A \sim 60$ for which large-scale nuclear shell model calculations, which — as we will show below — describe the GT$_+$ distribution quite well, can be performed.

3. For even higher densities nuclei with mass numbers $A > 65$, for which detailed shell model calculations are yet not possible due to computational limitations, become quite abundant. However, when this happens during the collapse the electron chemical potential is noticeably larger than the Q-value. As a consequence it might be sufficient for a reliable estimate of the capture rates to employ a nuclear model which describes the centroid and the total GT$_+$ strength reasonably well.

When Fuller, Fowler and Newman (FFN) [119, 135, 136, 137] did their pioneering calculations of stellar weak-interaction rates based on the independent particle model, only little experimental guidance existed; in particular, no experimental information about the GT$_+$ strength distribution was available. This situation then changed drastically when GT distributions, mainly due to the (p,n) work at the Indiana cyclotron [128] and to the (n,p) work performed at TRIUMF [109, 138, 139, 140], for several nuclei in the iron mass range became available. It had already become clear due to studies of sd-shell

nuclei [130], that a description of the GT distributions requires a careful consideration of nucleon-nucleon correlations and that the diagonalization shell model would be the method of choice to do the job. Although studies of mid-shell pf nuclei were initially prohibited by computational limitations, these could be overcome by the development of new codes like ANTOINE by Etienne Caurier and by growing computer power. Finally, Caurier *et al.* then performed large-scale shell model calculations for nuclei in the iron mass range which indeed reproduced the available experimental GT_- and GT_+ data quite well [141]. Furthermore, these studies also described the low-energy nuclear spectra well. In summary, the study of Caurier *et al.* implied that the shell model was indeed the tool to calculate the weak-interaction rates as needed for late-stage presupernova core evolution for which the stellar composition is dominated by nuclei with mass numbers $A = 45-65$ [141]. This task has been executed in [120] where the rates for electron and positron captures and for β^+ and β^- decays have been calculated for stellar conditions and for more than 100 nuclei in the mass range $A = 45 - 65$. The rates are based on the explicite evaluation of the GT distributions for the lowest energy states of each nucleus, supplemented by the contributions of the 'back-resonances'. Calculated energies or GT transition strengths have been replaced by experimental data whenever possible. In recent years the shell model GT distributions have been stringently tested when the (d,^{2}He) GT_+ with an order of magnitude better energy resolution than the (n,p) data became available [134]. Although not perfect, the shell model results proved to be quite accurate. Comparisons of electron capture rates calculated with the experimental (d,^{2}He) and with the shell model GT_+ distributions (considering ground states only) generally agree within a factor of 2 at the relevant temperature and density regimes. Fig. 9 compares the shell model spectrum and GT_+ distribution for ^{51}V with the experimental data.

Fig. 10 compares the shell model and FFN electron capture rates for several nuclei at temperatures and densities which are typical for the core in late-stage presupernovae. Importantly the shell model rates are systematically smaller than the FFN rates with quite significant consequences for the presupernova and core-collapse evolutions, as is discussed below. The reasons for the differences between the FFN and shell model rates are discussed in [120]. They include differences in the systematics of nuclear pairing effects (which have been added empirically by FFN), but also improved experimental data which had not been available when FFN derived their seminal stellar weak-interaction rate tables. The differences between the FFN and shell model β_- rates are smaller than for electron capture and do not show a systematic tendency. Comparisons are presented in [143, 120].

To study the influence of the shell model rates on presupernova models Heger *et al.* [149, 104] have repeated the calculations of Weaver and Woosley [103] keeping the stellar physics, except for the weak rates, as close to the original studies as possible. Fig. 11 examplifies the consequences of the shell model weak interaction rates for presupernova models in terms of the three decisive quantities: the central Y_e value and entropy and the iron core mass. The central values of Y_e at the onset of core collapse increased by 0.01–0.015 for the new rates. This is a significant effect. We note that the new models also result in lower core entropies for stars with $M \leq 20M_\odot$, while for $M \geq 20M_\odot$, the new models actually have a slightly larger entropy. The iron core masses are generally smaller in the new models where the effect is larger for more massive stars ($M \geq 20M_\odot$), while for the most common supernovae ($M \leq 20M_\odot$) the reduction is by about 0.05 $M_\odot$.

Electron capture dominates the weak-interaction processes during presupernova evolution. However, as already anticipated by Aufderheide et al. [144], during silicon burning, β decay (which increases Y_e) can compete and adds to the further cooling of the star [149, 104]. With increasing densities, β-decays are hindered as the increasing Fermi energy of the electrons blocks the available phase space for the decay. Thus, during collapse β-decays can be neglected

We note that the shell model weak interaction rates predict the presupernova evolution to proceed along a temperature-density-Y_e trajectory where the weak processes are dominated by nuclei rather close to stability. Thus it will be possible, after radioactive ion-beam facilities become operational, to further constrain the shell model calculations by measuring relevant beta decays and GT distributions for

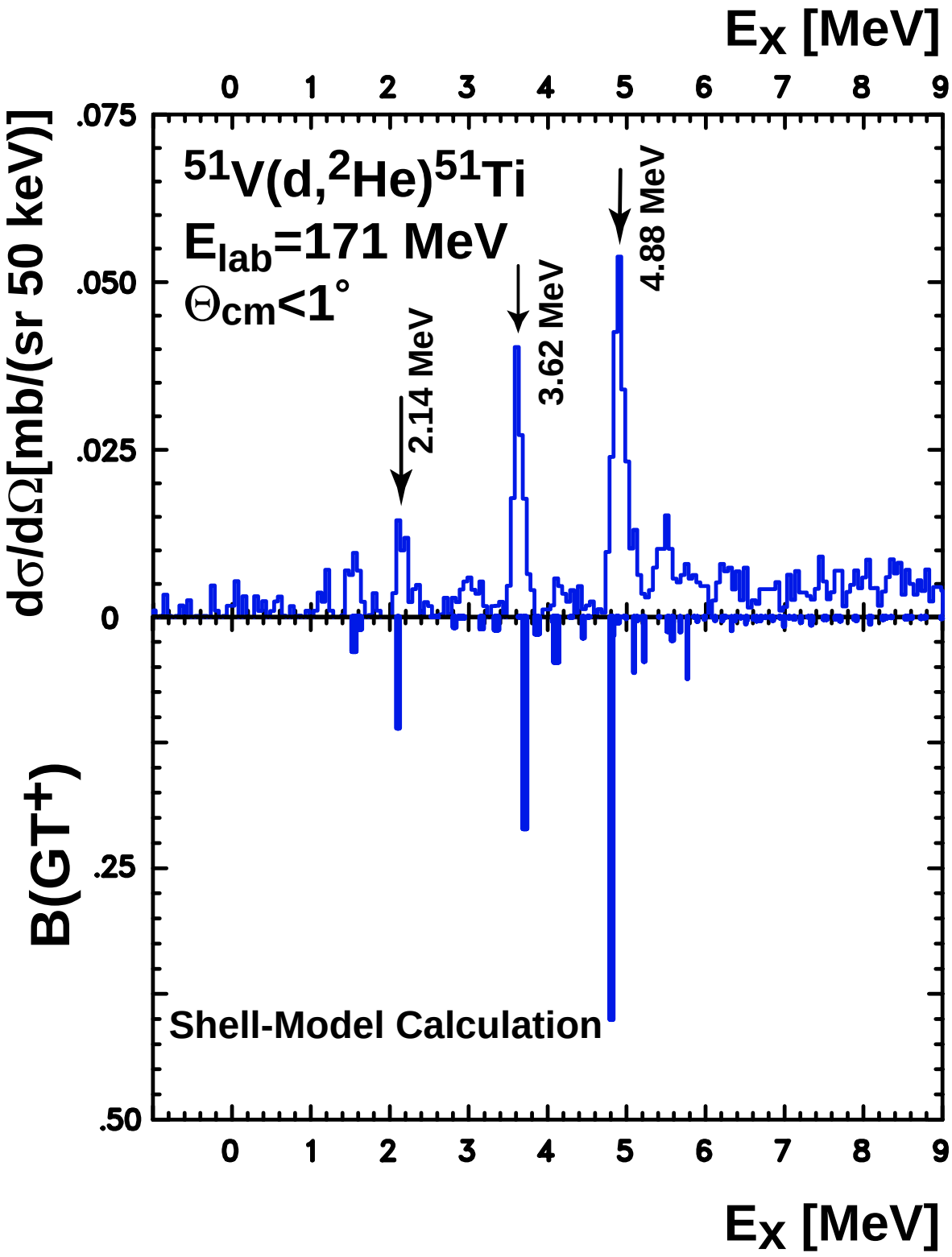

Figure 9: Comparison of the measured energy spectrum (left) and the ^{51}V(d,^{2}He)^{51}Ti cross section (right) at forward angles (which is proportional to the GT$_{+}$ strength) with the shell model predictions (the GT data are from [142]).

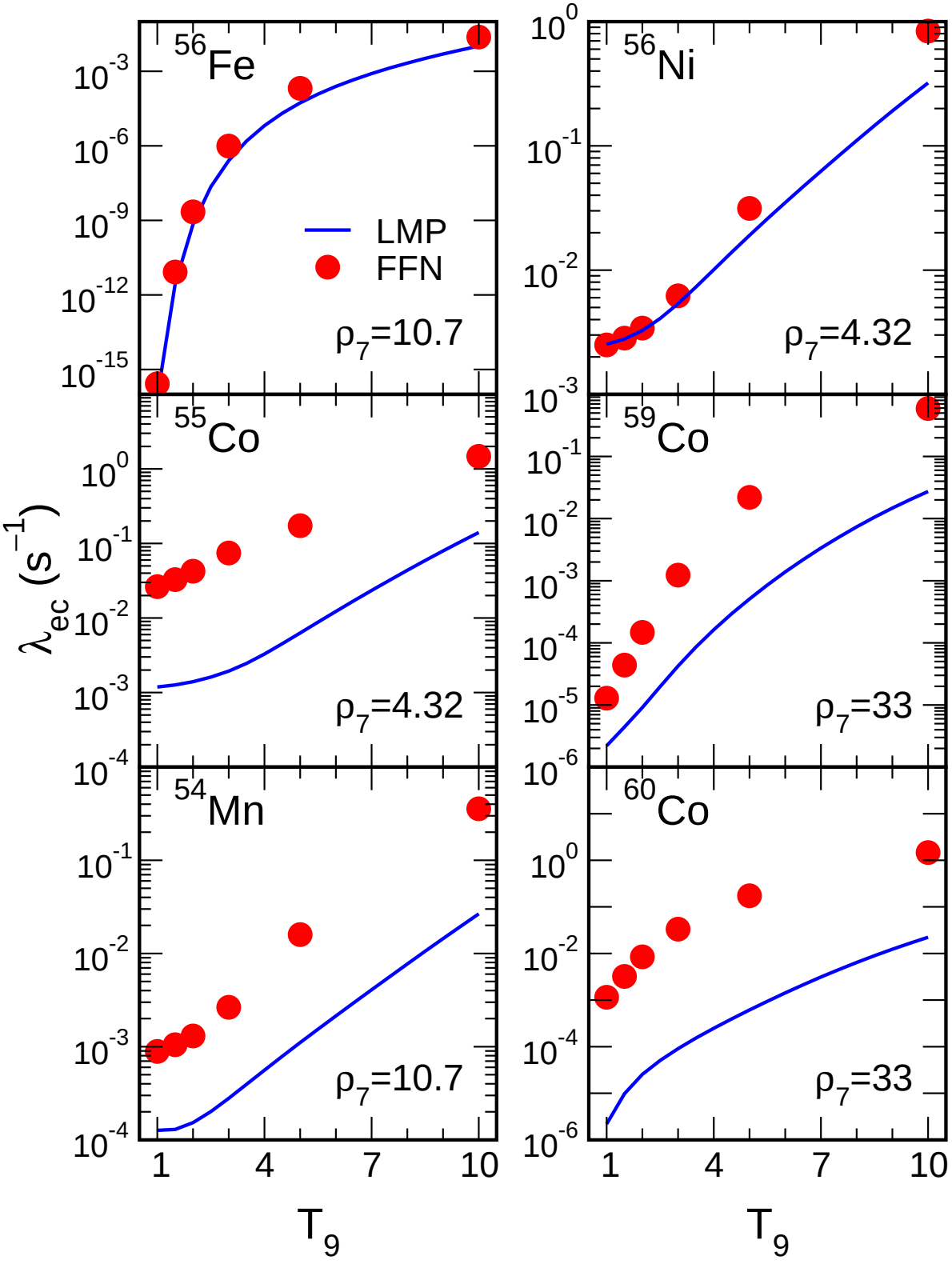

Figure 10: Shell model electron-capture rates as a function of temperature (T_9 measures the temperature in 10^9 K) and for selected densities (ρ_7 defines the density in 10^7 g cm^{-3}) and nuclei. For comparison, the FFN rates are given by the full points. (from [120])

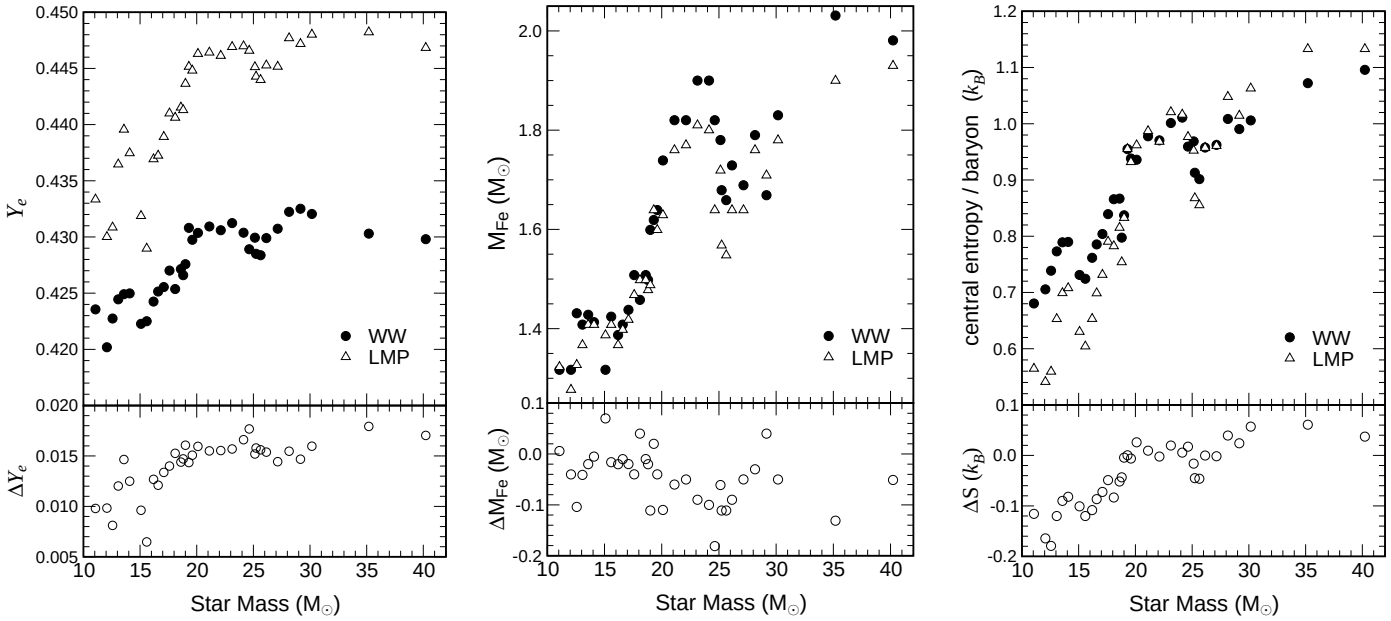

Figure 11: Comparison of the center values of Y_e (left), the iron core sizes (middle), and the central entropy (right) for $11 - 40M_\odot$ stars between the WW models, which used the FFN rates, and the ones using the shell model weak interaction rates (LMP) (from [104]).

unstable nuclei. Ref. [104] identifies those nuclei which dominate (defined by the product of abundance times rate) the electron capture and beta decay during various stages of the final evolution of a $15M_\odot$, $25M_\odot$ and $40M_\odot$ star.

The continuous electron captures in the core do not only reduce the electron-to-nucleon ratio, and hence the pressure which the electron degeneracy can stem against the gravitational collapse, it also shifts the nuclear composition in the core to more neutron-rich and heavier nuclei (see Figs. 5. As noted by Fuller, this tendency might significantly reduce the electron captures once nuclei with neutron numbers $N > 40$ are abundant [150]. The argument is based on the independent particle model (IPM): GT transitions can only proceed to the same nuclear orbital or to the spin-orbit partner in the same harmonic oscillator shell. Consequently, for nuclei with charge-numbers $Z < 40$, but neutron numbers $N > 40$ GT transitions are completely blocked by the Pauli principle within the independent particle model [43]. Hence it has been assumed for many years that electron captures during the collapse phase occur on free protons rather than on nuclei, although the abundance of free protons is noticeably smaller than the one of nuclei (e.g. [1]). However, the IPM picture is not applicable. At first, the core has a sizable finite temperature which can lead to thermal unblocking of GT transitions [152]. More importantly, the energy gap between the pf-shell ($f_{5/2}, p_{1/2}$) and the lowest orbital of the next (sdg) shell ($g_{9/2}$) is only 2–3 MeV. The residual interaction thus mixes nucleons in these orbitals leading to neutron holes in the pf-shell or to proton excitations to sdg (mainly $g_{9/2}$) orbitals. Both effects unblock GT_+ transitions. In fact, recent experiments have observed a non-vanishing GT_+ strength for ^{72}Ge and ^{76}Se [145] which should be exactly zero in the IPM.

An additional complication arizes for the calculation of the stellar electron capture rates due to the finite temperature of the core. At a typical core temperature of $T = 1$ MeV, the internal excitation energy of a nucleus with mass number $A \sim 80$ is about 8-10 MeV, i.e. much larger than the energy gap between the pf- and sdg-shells. Hence, one expects that at the stellar temperatures the unquenching of GT_+ transitions is more effective than for the ground state. Unfortunately, diagonalization shell model calculations, which have been successfully applied to the evaluation of electron capture rates for lighter (i.e. pure pf-shell) nuclei cannot be employed for the required multi-shell calculations due to the extreme

dimensions of the model spaces involved (for ^{72}Ge a calculation within the pf-sdg model space contains about 10^{24} configurations). To overcome this problem, a hybrid model has been suggested [146]. In the first step, the nucleus is described by a Slater determinant with temperature-dependent occupation numbers for the valence orbitals. These occupation numbers are determined within the Shell Model Monte Carlo (SMMC) approach which allows the calculation of thermally-averaged properties of nuclei in extremely large model spaces (here the full pf-sdg shells) and considering the relevant correlations among nucleons [147]. Although the SMMC allows in principle the calculation of GT strength distributions, such calculations are numerically quite challenging and usually enable only the determination of the first 2 moments of the distribution which is insufficient for the calculation of stellar electron capture rates [148]. Therefore, the capture rates are derived in a second step from the GT_+ strength distributions calculated within the Random Phase Approximation built on top of the temperature-dependent Slater determinant. Using the hybrid model, capture rates have been determined for about 200 nuclei and, combined with the rates for pf-shell nuclei [120], a rate table for the appropriate collapse temperatures, densities and Y_e values has been compiled.

The Random Phase Approximation (RPA) treats nucleon-nucleon correlations only on the 1-particle-1-hole level and hence misses higher-order correlations, which are considered within the shell model and which are important to reproduce details of the GT strength like fragmentation and the low-energy tail of the strength (which is particularly important for the calculation of β-decay rates). However, the RPA is known to give a reasonable account of the centroid of strength distributions as well as of the total GT_+ strength. Thus, one should be cautious to use the hybrid model for stellar conditions for which the electron chemical potential is similar to the nuclear Q-value as then the capture rate will be quite sensitive to the detailed GT_+ strength distribution (shell model and hybrid model rates can then easily deviate by factors 2–3 [151]). Luckily, $\mu_e \sim Q$ occurs at core densities at which the core composition is still dominated by nuclei $A \approx 55 - 65$ for which large-scale shell model rates exist [120]. At higher densities, when nuclei with $A > 65$, for which diagonalization shell model calculations are not possible and the capture rates have to be estimated by the hybrid model, are abundant, the electron chemical potentials is noticeably larger than the typical nuclear Q-values. Under these conditions capture rates are mainly sensitive to the centroid and the total strength of the GT_+ distributions which are reasonably well described within the RPA. At even higher densities, say $\rho > 10^{11}$ g/cm^3, the capture rates on nuclei become quite similar at larger densities, depending now basically only on the total GT strength, but not its detailed distribution. This is demonstrated in Fig. 12 which shows the hybrid model capture rates as function of Q-value at 3 different stellar conditions. The Q-value dependence of the capture rate for a transition from a parent state at excitation energy E_i to a daughter state at E_f ($\Delta E = E_f - E_i$) is well approximated by [137, 153]

$$\begin{aligned} \lambda(Q) &= \ln(2) 10^{-3.588} (kT/m_e)^5 |M_{GT}|^2 \\ &\times \ (F_4(\eta) - 2\chi F_3(\eta) + \chi^2 F_2(\eta)) \end{aligned} \tag{26}$$

where $\chi = (Q - \Delta E)/kT$, $\eta = U_F + m_e + Q - \Delta E$ and U_F is the kinetic electron chemical potential (the total includes the electron rest mass m_e). The quantities F_k are the relativistic Fermi integrals of order k.

Thus, finite temperature and correlations unquench the GT_+ strength noticeably. As electrons have to overcome a larger threshold for neutron-rich nuclei than for protons, the electron capture rate on individual nuclei is smaller than on free protons. However, what matters is the product of abundance times capture rate. As nuclei are much more abundant in the collapsing core, due to its small entropy of order 1 k_B per nucleon, than protons, electron capture on nuclei clearly dominates as is shown in Fig. 13.

It is also important to stress that electron capture on nuclei and on free protons differ quite noticeably in the neutrino spectra they generate. Fig. 13 demonstrates that capture on nuclei having a mean energy

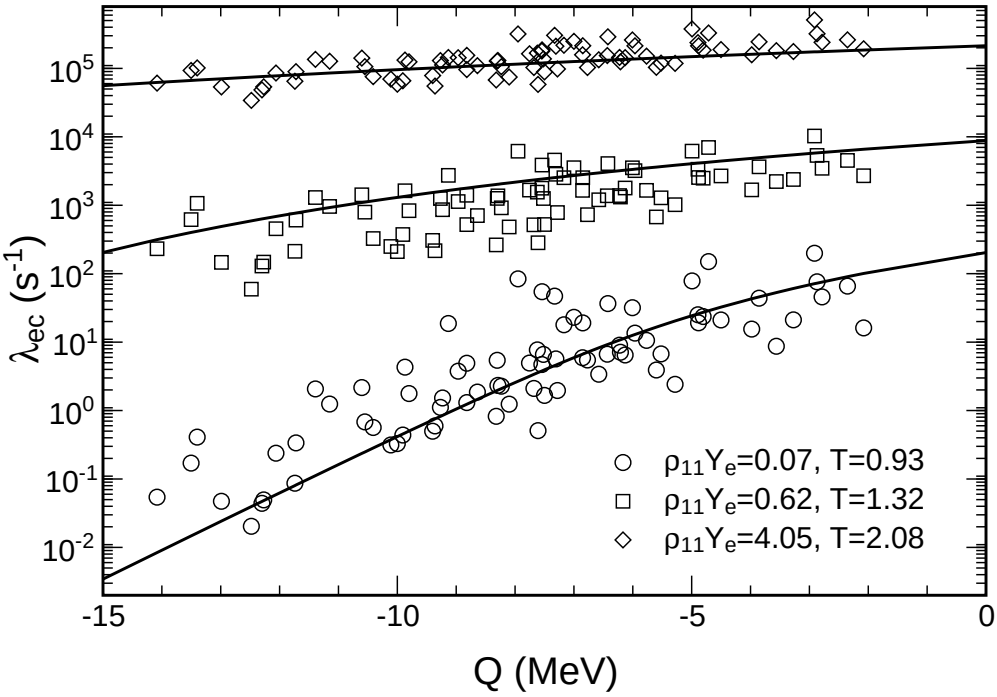

Figure 12: Electron capture rates on nuclei as function of Q-value for three different stellar conditions. Temperature is measured in MeV. The solid lines represent the approximate Q-dependence of the rates as defined in Eq. (26). (from [153])

40-60% less than that produced by capture on protons. These differences are quite relevant as neutrino-matter interactions, which scale with the square of the neutrino energy E_ν, are essential for the collapse simulations. Although capture on nuclei under stellar conditions involves excited states in the parent and daughter nuclei, it is mainly the larger Q-value which significantly shifts the energies of the emitted neutrinos to smaller values.

The effects of this more realistic implementation of electron capture on heavy nuclei have been evaluated in independent self-consistent neutrino radiation hydrodynamics simulations by the Oak Ridge and Garching collaborations [153, 154, 155]. The changes compared to the previous simulations, which adopted the IPM rate estimate from Ref. [43] and hence basically ignored electron capture on nuclei, are significant. Fig. 14 shows a key result: in denser regions, the additional electron capture on heavy nuclei results in more electron capture in the new models. In lower density regions, where nuclei with $A < 65$ dominate, the shell model rates [120] result in less electron capture. The results of these competing effects can be seen in the first panel of Figure 14, which shows the distribution of Y_e throughout the core at bounce (when the maximum central density is reached). The combination of increased electron capture in the interior with reduced electron capture in the outer regions causes the shock to form with 16% less mass interior to it and a 10% smaller velocity difference across the shock. In spite of this mass reduction, the radius from which the shock is launched is actually displaced slightly outwards to 15.7 km from 14.8 km in the old models. Also the altered gradients in density and lepton fraction play an important role in the behavior of the shock. Though also the new models fail to produce explosions in the spherically symmetric case, the altered gradients allow the shock in calculations with improved capture rates to reach a somewhat larger maximum radius than in the old models.

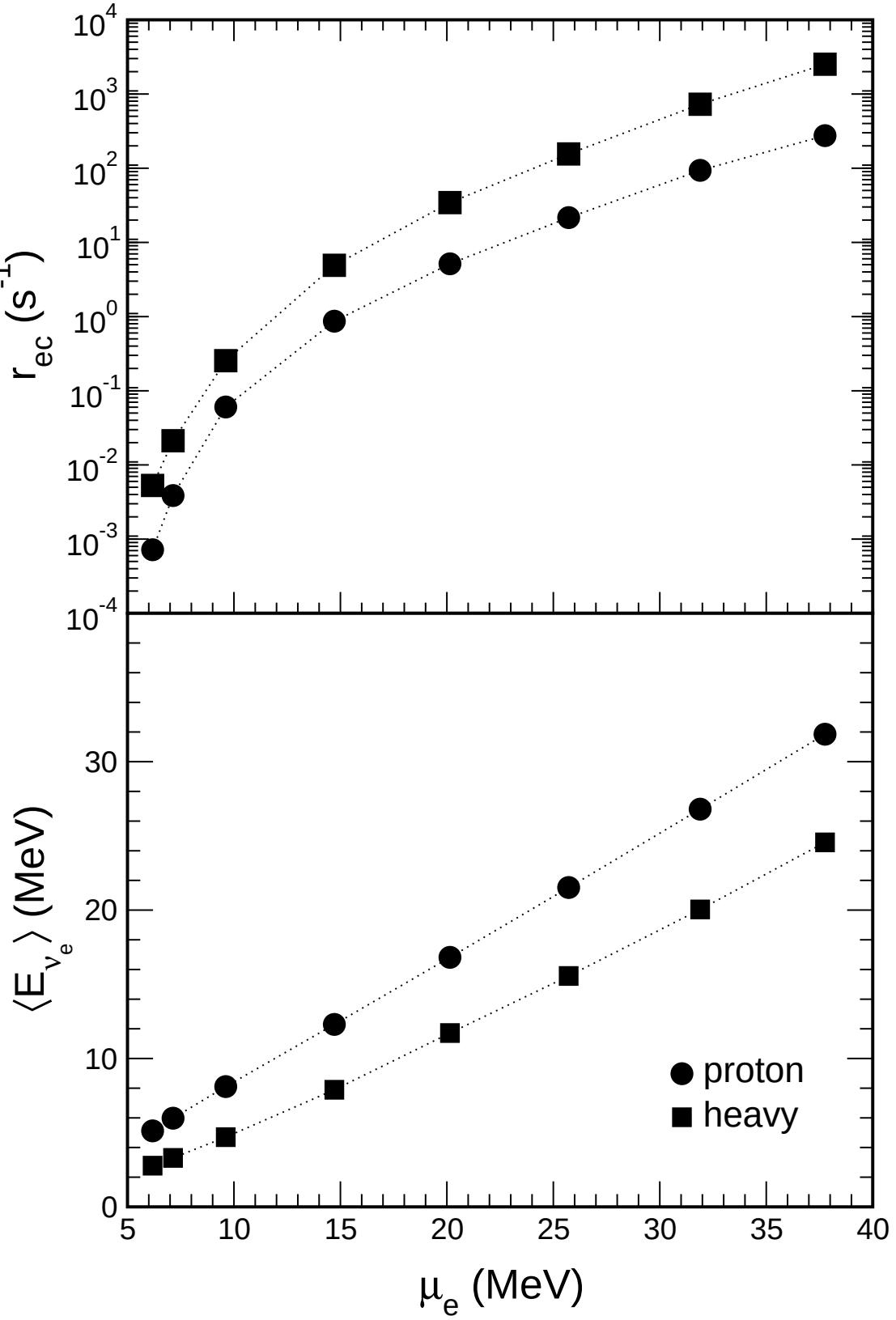

Figure 13: The upper panel compares the products of number abundances and electron capture rates for free protons (r_p, circles) and nuclei (r_h), squares) as functions of electron chemical potential along a stellar collapse trajectory. The lower panel shows the related average energy of the neutrinos emitted by captures on nuclei and protons. The results for nuclei are averaged over the full nuclear composition. (from [153])

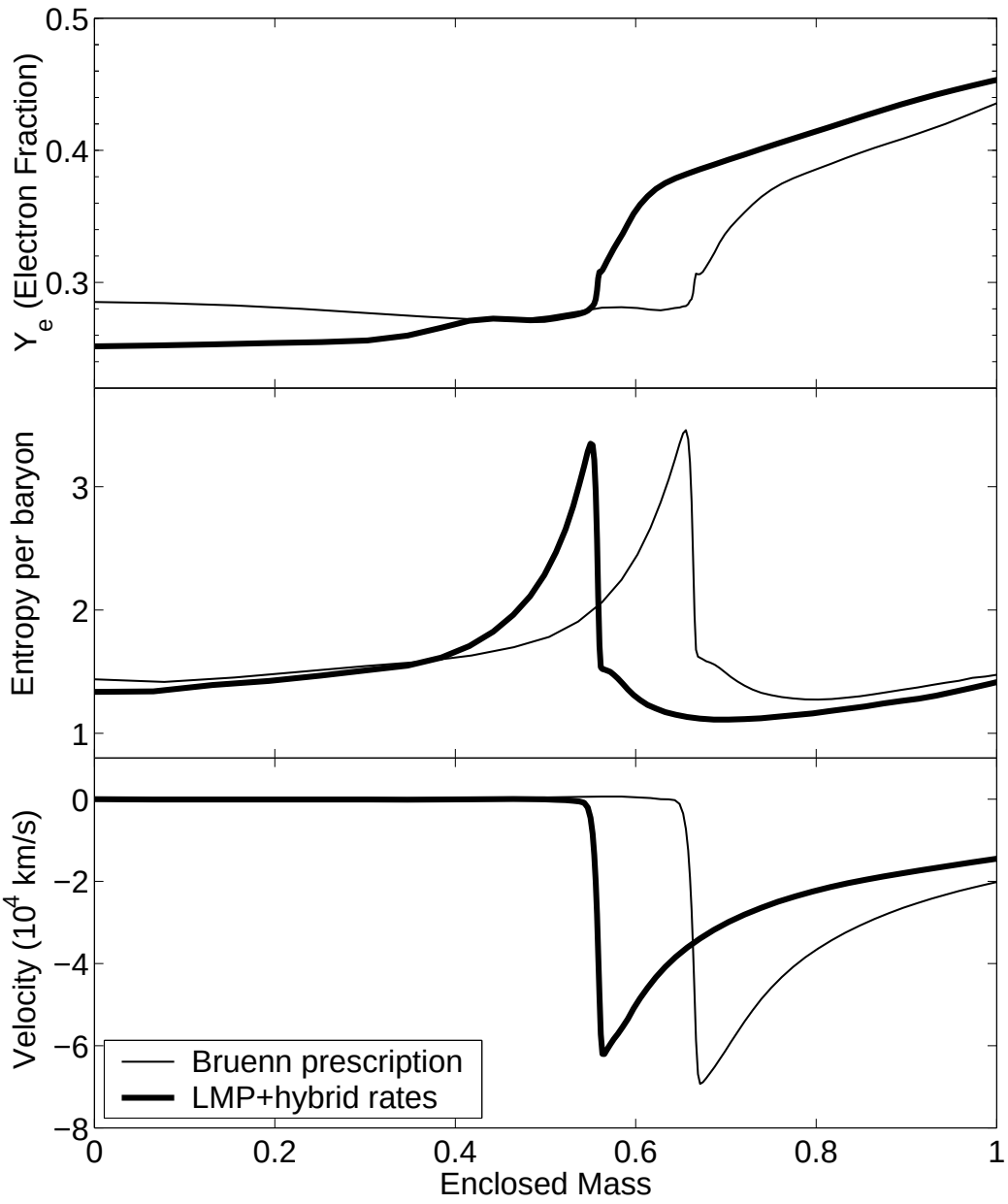

Figure 14: The electron fraction, entropy, and velocity as functions of the enclosed mass at bounce for a 15 solar mass model [154]. The thin line is a simulation using the Bruenn parameterization while the thick line is for a simulation using the LMP and Hybrid reaction rate sets (from [154]).

2.3 Inelastic neutrino-nucleus scattering

While the neutrinos can leave the star unhindered during the presupernova evolution, neutrino-induced reactions become more and more important during the subsequent collapse stage due to the increasing matter density and neutrino energies; the latter are of order a few MeV in the presupernova models, but increase roughly approximately to the electron chemical potential [43]. Coherent and conservative neutrino scattering off nuclei and scattering on electrons are the two most important neutrino-induced reactions during the collapse. The first reaction randomizes the neutrino paths out of the core and, at densities of about 10^{12} g/cm^3, the neutrino diffusion timescale gets larger than the collapse time; the neutrinos are trapped in the core for the rest of the contraction. Scattering off electrons and neutrino emission and reabsorption then establishes thermal equilibrium between the trapped neutrinos and the stellar matter rather quickly. The inner core with trapped neutrinos collapses with conserved lepton number and adiabatically as a homologous unit until it reaches densities slightly in excess of nuclear matter, generating a bounce and launching the supernova shock wave.

Neutrino-induced reactions on nuclei, other than coherent scattering, can also play a role during the collapse and the subsequent explosion phase [156]. Note that during the collapse only ν_e neutrinos are present. Thus, charged-current reactions $A(\nu_e, e^-)A'$ are strongly blocked by the large electron chemical potential [157, 158]. Inelastic neutrino scattering on nuclei can compete with $\nu_e + e^-$ scattering at higher neutrino energies $E_\nu \geq 20$ MeV [157]. Here the cross sections are mainly dominated by first-forbidden transitions. Finite-temperature effects play an important role for inelastic $\nu + A$ scattering below $E_\nu \leq 10$ MeV. This comes about as nuclear states get thermally excited which are connected to the ground state and low-lying excited states by modestly strong GT transitions and increased phase space. As a consequence the cross sections are significantly increased for low neutrino energies at finite temperature and might be comparable to $\nu_e + e^-$ scattering [159]. Thus, inelastic neutrino-nucleus scattering, which until very recently has been neglected in collapse simulations, should be implemented in such studies. A first result of such an implementation is given below.

Currently no data for inelastic neutral-current neutrino-nucleus cross sections are available for supernova-relevant nuclei ($A \sim 60$). However, as has been demonstrated in [160], precision M1 data, obtained by inelastic electron scattering, supply the required information about the Gamow-Teller GT$_0$ distribution which determines the inelastic neutrino-nucleus cross sections for supernova neutrino energies. The argumentation is built on the observation that for M1 transitions the isovector part dominates and the respective isovector M1 operator is given by

$$\mathcal{O}_{iv} = \sqrt{\frac{3}{4\pi}} \sum_k \left[\mathbf{l}(k)\mathbf{t_z}(k) + 4.706\sigma(k)\mathbf{t_z}(k) \right] \mu_N \tag{27}$$

where the sum is over all nucleons and μ_N is the nuclear magneton, and that the spin part of the isovector M1 operator is proportional to the desired zero-component of the GT operator. Thus, experimental M1 data yield the needed GT$_0$ information to determine supernova neutrino-nucleus cross sections, to the extent that the isoscalar and orbital pieces present in the M1 operator can be neglected. First, it is wellknown that the major strength of the orbital and spin M1 responses are energetically well separated. Furthermore, the orbital part is strongly related to deformation and is suppressed in spherical nuclei, like ^{50}Ti, ^{52}Cr, ^{54}Fe. These nuclei have the additional advantage that M1 response data exist from high-resolution inelastic electron scattering experiments [161]. Satisfyingly, large-scale shell model calculations reproduce the M1 data quite well, even in details [160]. The calculation also confirms that the orbital and isoscalar M1 strengths are much smaller than the isovector spin strength. Thus, the M1 data represent, in a good approximation, the needed GT$_0$ information (upto a known constant factor). Fig. 15 compares the inelastic neutrino-nucleus cross sections for the 3 studied nuclei, calculated from the experimental M1 data and from the shell model GT$_0$ strength. The agreement is quite satisfactory. It is further improved, if one corrects for possible M1 strength outside of the explored experimental

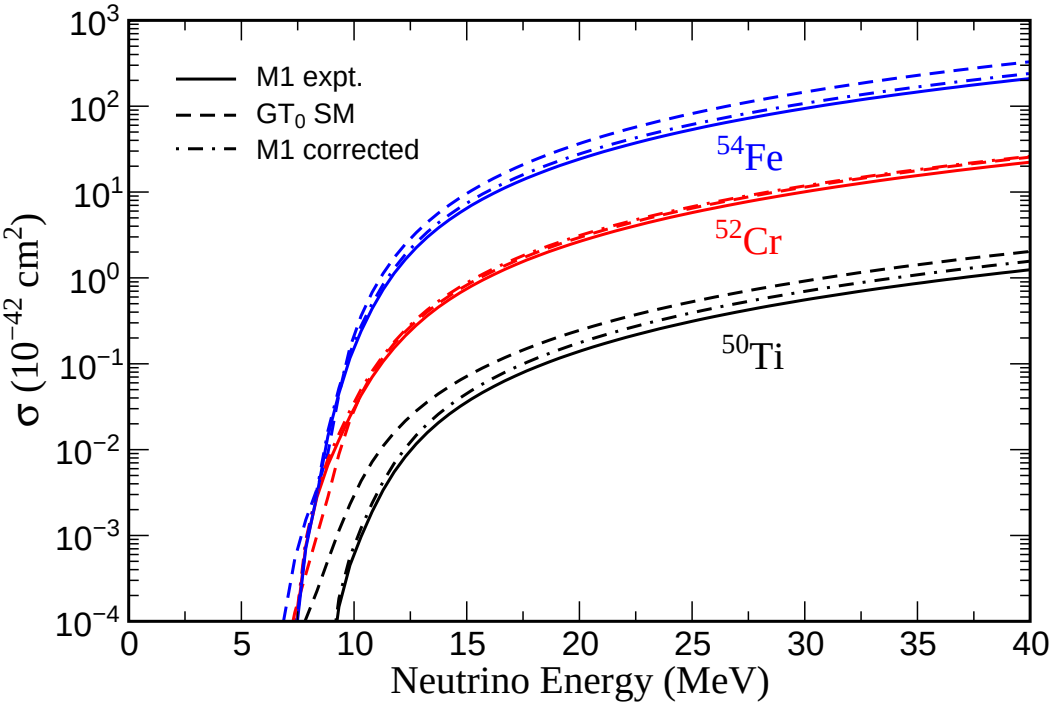

Figure 15: Neutrino-nucleus cross sections calculated from the M1 data (solid lines) and the shell-model GT_0 distributions (dotted) for ^{50}Ti (multiplied by 0.1), ^{52}Cr, and ^{54}Fe (times 10). The long-dashed lines show the cross sections from the M1 data, corrected for possible strength outside the experimental energy window. (from [160])

energy window. Also differential neutrino-nucleus cross sections as functions of initial and final neutrino energies, calculated from the M1 data and the shell model, agree quite well [160]. On the basis of this comparison, one can conclude that the shell model is validated for the calculations of inelastic neutral-current supernova neutrino-nucleus cross sections. This model can then also be used to calculate these cross sections at the finite temperature in the supernova environment [160]. Juodagalvis et al. have calculated double-differential inelastic neutrino-nucleus cross sections for many nuclei in the $A \sim 56$ mass range, based on shell model treatment of the GT transitions and on RPA studies of the forbidden contributions [162]. A detailed table of the cross sections as function of initial and final neutrino energies and for various temperatures is available from the authors of [162].

Although inelastic neutrino-nucleus scattering contributes to the thermalization of neutrinos with the core matter, the inclusion of this process has no significant effect on the collapse trajectories. However, it increases noticeably the opacity for high-energy neutrinos after the bounce. As these neutrinos excite the nuclei, they are down-scattered in energy, in this way significantly reducing the high-energy tail of the spectrum of emitted supernova neutrinos (see Fig. 16, [163]). This makes the detection of supernova neutrinos by earthbound detectors more difficult, as the neutrino detection cross section scales with E_ν^2.

3 Nucleosynthesis in proton-rich supernova ejecta

During the supernova explosion the shells of the star outside the so-called mass cut are ejected. In this way the elements that have been produced during the various stellar burning stages are mixed into the Interstellar Medium. In fact, core-collapse supernovae are the main contributors of the heavy elements ($A \geq 12$) in the Universe. For in-depth reviews of nucleosynthesis we refer to the work of Woosley and collaborators [103, 164], and to [165]. These authors also discuss the effect of the

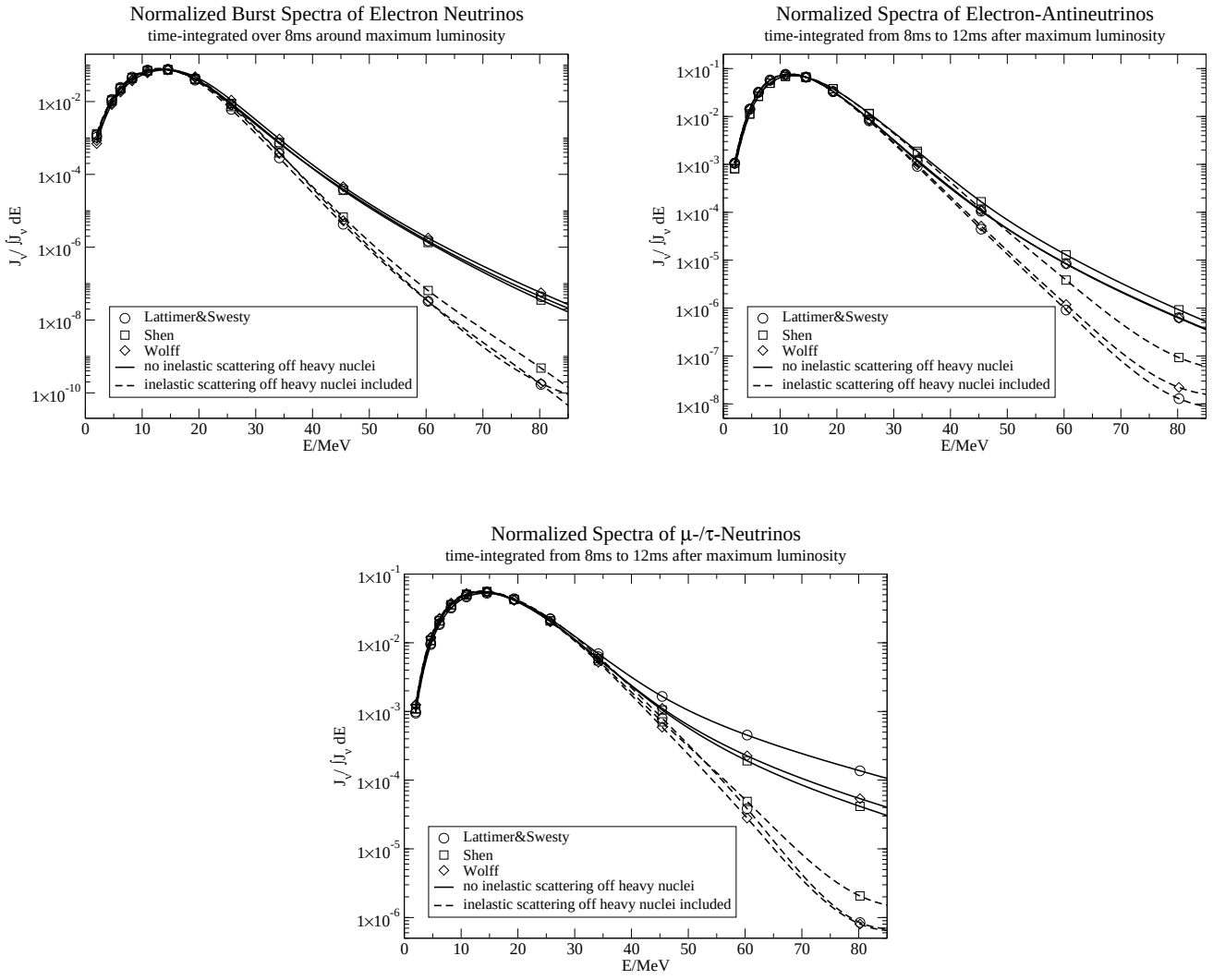

Figure 16: Comparison of the normalized spectra of ν_e, $\bar{\nu}_e$, and $\nu_{\mu,\tau}$ emitted in a time interval around the ν_e breakout burst shortly after bounce, without (solid) and with (dashed) consideration of inelastic neutrino-nucleus scattering in supernova simulations with the L&S (open circles), Shen (open squares), and Wolff (open diamonds) equations of state (see Sect. 2.1). The flattening of the dashed lines near the high-energy end of the plotted spectra is a consequence of the limited energy range of the available rate table for inelastic neutrino-nuclei scatterings and of disregarding these reactions at higher neutrino energies. (from [163]).

explosion on the nucleosynthesis, as the heating of the material induced by the passage of the shock wave gives rise to a short period of very fast (explosive) nuclear reactions which affects in particular the abundances of elements in the deeper stellar layers. For many years it has been customary to simulate the explosion and the effects of the shock wave by igniting a thermal bomb in the star's interior or by initiating the explosion by a strong push with a piston. But recently it has become possible [168, 169, 170, 179] to study the explosive nucleosynthesis using large nuclear networks coupled to stellar trajectories obtained in state-of-the-art supernova simulations with sophisticated, energy-dependent neutrino transport [166, 167] (see also Sect. 1.1)[4]. These studies have provided new insights into the explosive nucleosynthesis and its time evolution, and have led to the discovery of a novel nucleosynthesis process (the νp-process) [172, 179, 173], which we will briefly summarize in this section.

Due to the strong neutrino heating near the newly-formed neutron star, the ejected matter from the deepest layers of a supernova has temperatures $T_9 > 5$ and is dissociated into free protons and neutrons. These building blocks are assembled to nuclei when the matter moves outwards to cooler regions. This nucleosynthesis process and its final elemental abundances depend on outflow parameters like the expansion timescale, the entropy, and the Y_e value of the matter. As the ejection occurs in extreme neutrino fluences, Y_e is determined by the competition of electron neutrino and antineutrino absorption on neutrons and protons (Eqs. 1 and 2), respectively. In a rough approximation, the electron fraction that results from the competition of these neutron destroying and producing reactions can be expressed by

$$Y_e \sim \left[1 + \frac{L_{\bar{\nu}_e}\langle\epsilon_{\bar{\nu}_e}\rangle}{L_{\nu_e}\langle\epsilon_{\nu_e}\rangle}\right]^{-1} \quad , \tag{28}$$

where $\langle\epsilon\rangle$ and L are the average energy and the luminosity of the neutrinos or antineutrinos [174, 175]. Although this expression is rather crude and does not take into account a number of important effects and corrections, it is still good to capture the basic influence of neutrino and antineutrino absorptions in setting the neutron-to-proton ratio in the outflow[5]. As anticipated by Qian and Woosley [175], modern supernova simulations show that the early ejecta are proton-rich ($Y_e > 0.5$), while matter ejected later may become neutron-rich, potentially leading to r-process nucleosynthesis ([176, 177, 178] and references therein). This might happen seconds later in the baryonic outflow that is driven off the surface of the nascent neutron star by the strong heating of neutrinos radiated from the neutrinosphere. As the expanding neutron-rich matter in this so-called 'neutrino-driven wind' cools, nucleons recombine to α particles, some of which can at even lower temperatures assemble to ^{12}C by the reaction sequence $\alpha(\alpha\mathrm{n},\gamma)^9\mathrm{Be}(\alpha,\mathrm{n})^{12}\mathrm{C}$. The carbon nuclei will then capture additional α particles and neutrons until iron group nuclei are formed. If free neutrons are left and the number of neutrons per nucleus is high, the nuclei can act as "seed" for the formation of very heavy elements by subsequent r-processing in the high-entropy environment of the neutrino-wind (see Fig. 1, bottom right panel).

The early, proton-rich ejecta consist of two components. On the one hand there is material that comes from the convecting postshock region and is expelled when the explosion is launched and the shock accelerates ('hot bubble ejecta'). Much of this material starts a rather slow expansion from large distances from the neutrino-radiating neutron star, is quite dense, has modest entropies ($s \sim 15 - -30\,k_\mathrm{B}$ per nucleon), and is slightly neutron-rich ($Y_e \gtrsim 0.47$) or moderately proton-rich with $Y_e \lesssim 0.52$ [179] (see Fig. 17). This material experiences little effect from neutrino-interactions during nucleosynthesis. This is in strong contrast to the matter ejected in the second component that contributes, which is the early neutrino-driven wind (Fig. 18). The wind comes from the surface of the hot neutron star, is strongly heated by neutrinos, and has to make its way out of the deep gravitational well of the compact

[4]Successful explosions were obtained in these simulations by slight modifications of governing parameters. This, however, did not modify the essential physics that determines the nucleosynthesis-relevant neutron-to-proton ratio in the ejecta.

[5]Fröhlich *et al.* [168], however, argue that in the early postbounce phase the inverse reactions of Eqs. (1) and (2) cannot be ignored and are in fact more important for setting the asymptotic Y_e-values of the outflowing material.

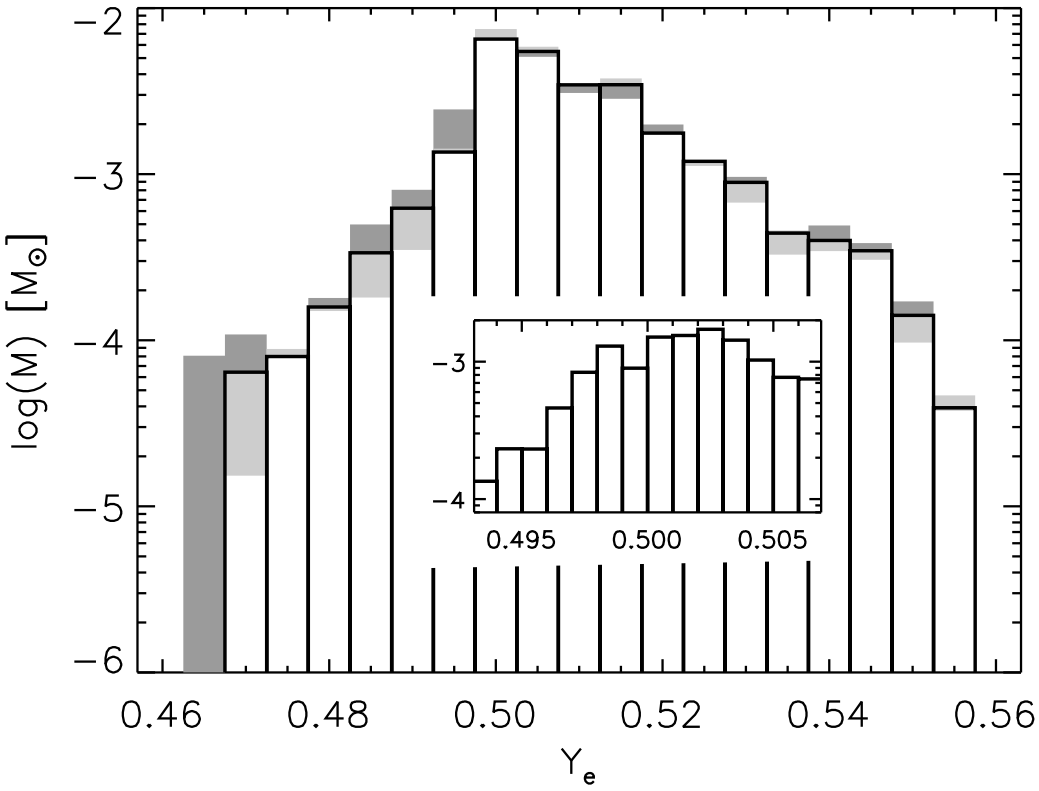

Figure 17: Ejecta mass versus Y_e of neutrino-heated and processed matter during the convective phase until $\sim$470 ms post bounce in a 2D simulation of the explosion of a 15 $M_\odot$ star [11]. The plot includes 'hot bubble ejecta' as well as some contribution from very early neutrino-wind material. The insert shows the region around $Y_e \sim 0.5$ in higher resolution. The grey shading indicates estimated errors due to the limited spatial resolution of the two-dimensional simulation (for details, see [11]; figure taken from [169]).

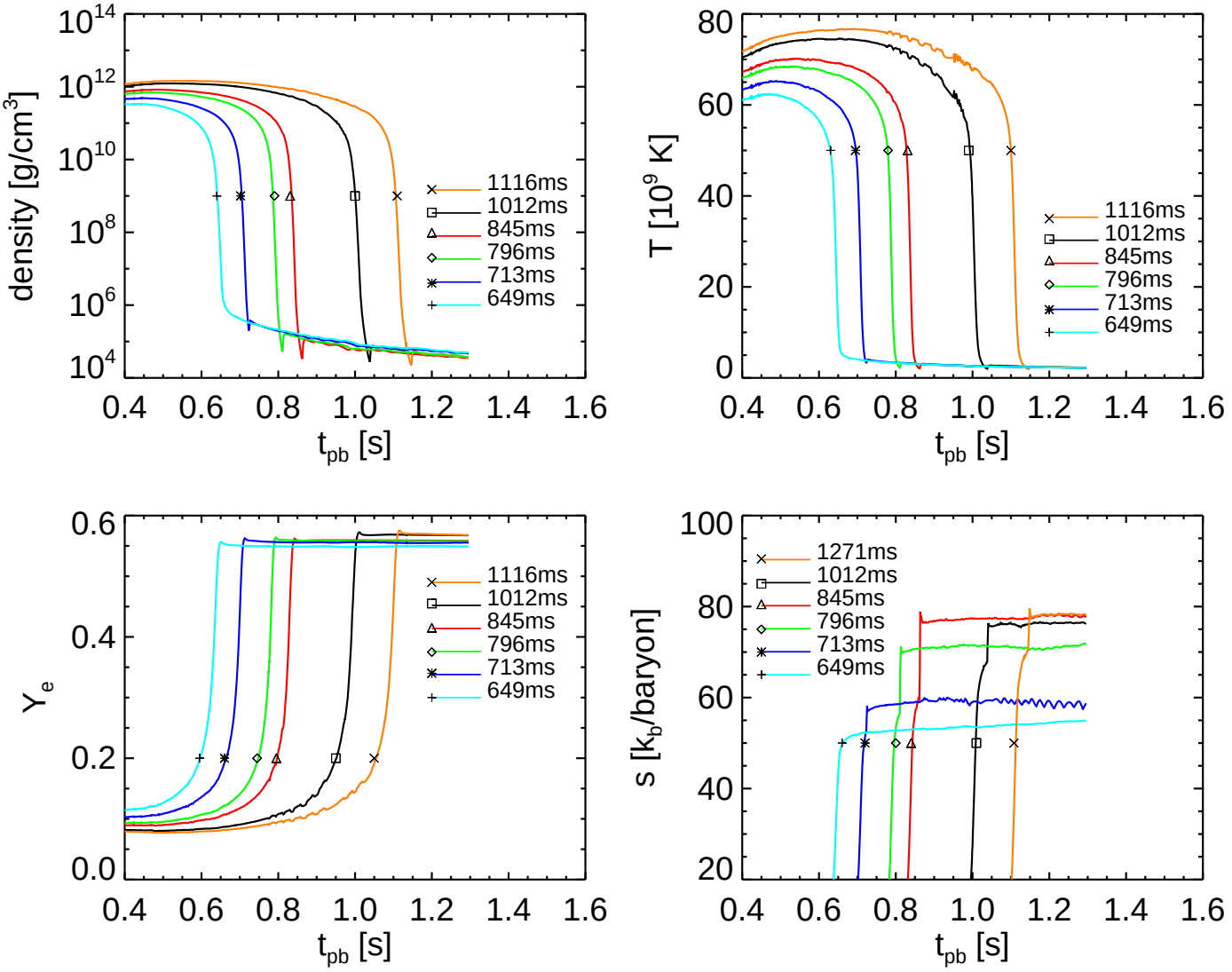

Figure 18: Density, temperature, Y_e, and entropy as functions of postbounce time along the trajectories of mass elements ejected in the early neutrino-driven wind of the 15 $M_\odot$ explosion of Fig. 17. The mass cut in this model develops around an enclosed baryonic mass of 1.41 $M_\odot$. The elements first follow the rise of temperature and density in the outer layers of the contracting neutron star and then enter a phase of very rapid expansion when they are ejected in the neutrino-driven wind. The curves are labeled by the time the mass elements cross a radius of 100 km. The collision with the slower preceding ejecta occurs through a wind termination shock and is visible as a non-monotonicity of the density and temperature, associated with an entropy increase of 10–15 k_B per nucleon (figure taken from [169]).

remnant. Therefore the wind has rather high entropies, short expansion timescales and can become quite proton-rich ($Y_e \sim 0.57$, [169, 170]).

Moving into cooler regions, protons and neutrons in this wind matter assemble first into ^{12}C and then, by a sequence of (p,γ), (α,γ) and (α,p) reactions into even-even $N = Z$ nuclei like ^{56}Ni, ^{60}Zn and ^{64}Ge, with some free protons left, and with enhanced abundances of ^{45}Sc, ^{49}Ti and ^{64}Zn solving a longstanding nucleosynthesis puzzle [169, 170]. In the absence of a sizable neutrino fluence, this nucleosynthesis sequence resembles explosive hydrogen burning on the surface of an accreting neutron star in a binary (the rp-process, [171]) and matter flow would basically end at ^{64}Ge as this nucleus has a β halflive (≈ 64 s) which is much longer than the expansion timescale and proton captures are prohibited by the small reaction Q value. However, the wind material is ejected in the presence of an extreme flux of neutrinos and antineutrinos. While ν_e-induced reactions have no effect as all neutrons are bound in nuclei with rather large neutron separation energies, antineutrino absorption on the free protons yield a continuous supply of free neutrons with a density of free neutrons of 10^{14}–10^{15} cm^{-3} for several seconds, when the temperatures are in the range 1–3 GK [172]. These neutrons, not hindered by Coulomb repulsion, are readily captured by heavy nuclei in a sequence of (n,p) and (p,γ) reactions in this way effectively by-passing the nuclei with long beta-halflives like ^{64}Ge and allowing the matter flow to proceed to heavier nuclei (see Fig. 19).

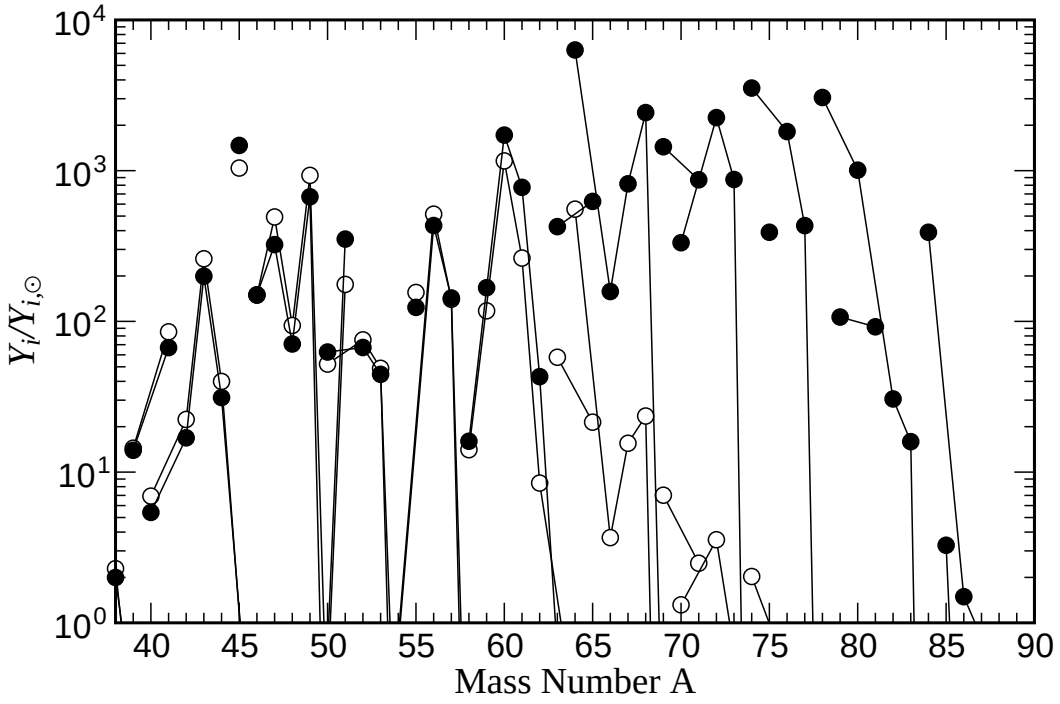

Figure 19: Elemental abundance yields (normalized to solar) for elements produced in the proton-rich environment shortly after the supernova shock formation. The matter flow stops at nuclei like ^{56}Ni and ^{64}Ge (open circles), but can proceed to heavier elements if neutrino reactions are included during the network (full circles); figure from [170].

Fröhlich *et al.* argue that all core-collapse supernovae will eject hot, explosively processed matter subject to neutrino irradiation and that this novel nucleosynthesis process (called νp-process) will operate in the innermost ejected layers producing neutron-deficient nuclei above $A > 64$ [172]. However, how far the mass flow within the νp-process can proceed, strongly depends on the environment conditions, most noteably on the Y_e value of the matter [179, 170, 173]. Obviously the larger Y_e, the larger the abundance of free protons which can be transformed into neutrons by antineutrino absorption. (The reservoir of free neutrons is also larger if the luminosities and average energies of antineutrinos are larger

or the wind material expands more slowly.) Figure 20 shows the dependence of the νp-process abundances on the Y_e value of the ejected matter (similar results are presented in [179, 173]). Nuclei heavier than $A = 64$ are only produced for $Y_e > 0.5$, showing a very strong dependence on Y_e in the range 0.5–0.6. A clear increase in the production of the light p-nuclei, ^{92,94}Mo and ^{96,98}Ru, is observed as Y_e gets larger. Thus the νp process offers the explanation for the production of these light p-nuclei, which was yet unknown. However, simulations fail to reproduce the observed abundance of ^{92}Mo, the most abundant p-nucleus in nature, which might be related to current uncertainties in the nuclear physics involved [179]. It is, however, observed that ^{92}Mo is significantly enhanced in slightly neutron-rich winds with Y_e values between 0.46 and 0.49 as they might be found in a later phase of the explosion (a few seconds after bounce) [173]. Here the α-rich freeze-out overabundantly produces ^{90}Zr from which some matter flow is carried to ^{92}Mo by successive proton captures [179, 173]. The νp process might also explain the presence of strontium in the extremely metal-poor, and hence very old, star HE 1327-2326 [180].

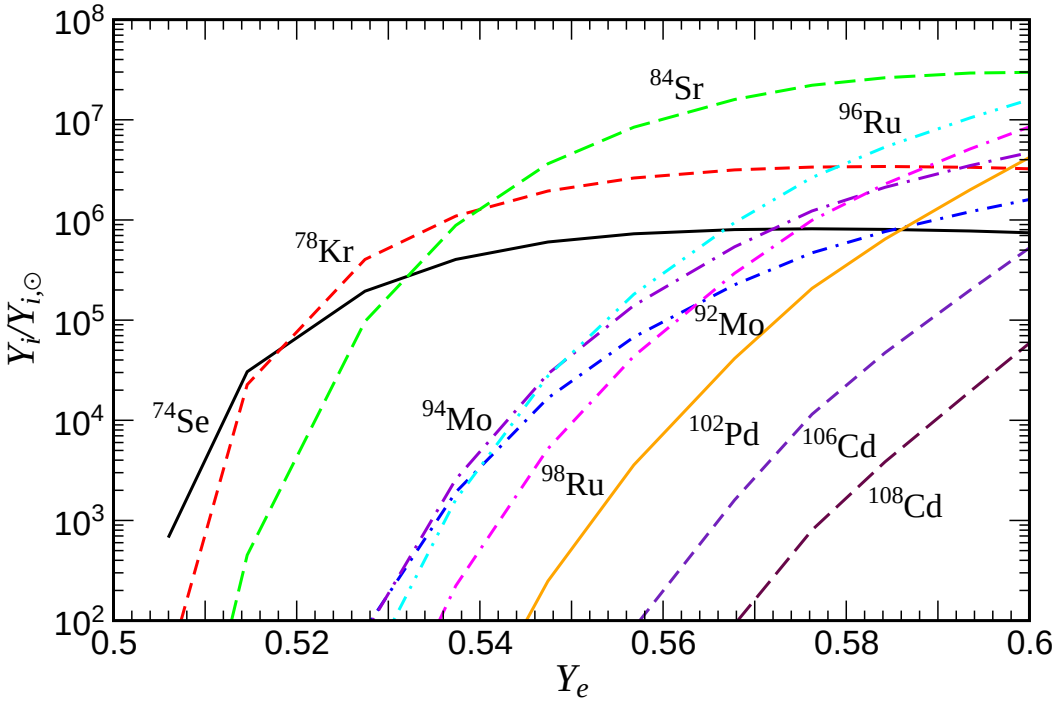

Figure 20: Light p-nuclei abundances in comparison to solar abundances as functions of Y_e. The Y_e-values given are the ones obtained at a temperature of 3 GK that corresponds to the moment when nuclei are just formed and the νp-process starts to act (from [170]).

4 Conclusions

Where does supernova research stand some 15 years after Hans Bethe's seminal review [1]? This review was already inspired by the once-in-a-hundred-years event of Supernova 1987A, the closest supernova for more than 300 years and certainly the best observed one ever. Not only did SN1987A impressively confirm our general picture of stellar core collapse and neutron star birth by the historical detection of two dozens of the emitted neutrinos. It also provided us with unambiguous evidence for the importance of hydrodynamic instabilities during the explosion, which triggered large-scale radial mixing in the star and destroyed the spherical onion-shell structure of chemical composition layers in the progenitor star.

But it was not clear at the time Hans Bethe wrote his paper, how strongly this observation was linked to the processes in the deep interior of the star and causal for the explosion.

Most of the general ideas and concepts outlined in Hans Bethe's review are of fundamental relevance and therefore have retained their validity. Better numerical models and progress in theoretical understanding, however, have sharpened our view of many of the ingredients that play a role in stellar explosions. In fact, these most powerful and most violent explosive events in the universe turn out to be more fascinating and richer the closer we look.

New horizons were opened by the discovery of extremely energetic explosions of massive stars, so-called hypernovae, in connection with long-duration gamma-ray bursts (for a recent review on this subject, see [5]). In the collapsar model [181, 182], the production of a gamma-ray burst is linked to the collapse of a rapidly rotating massive star, in whose core a black hole is formed and disk accretion releases the energy that drives a pair of ultrarelativistic jets along the rotation axis. These jets are responsible for the production of the gamma-ray burst and its afterglow. The major part of the released energy powers the off-axis ejection of nonrelativistic material in the hypernova explosion. While this scenario applies only for a small fraction of stellar core collapses, it defines the factors that might discriminate events leading to hypernovae from those producing ordinary supernovae: massive stellar iron cores, black hole formation, very rapid rotation, and the build-up of strong magnetic fields in an accretion disk on the one hand and smaller cores, neutron star formation, slow rotation, and possibly a non-magnetohydrodynamic explosion mechanism on the other. Nature, of course, may differentiate less strictly and might produce a variety of intermediate events in which a combination of processes is at work.

The neutrino-driven explosion mechanism, originally proposed by Colgate & White [183], discovered in its modern version by Wilson [31], casted into a framework of equations that capture its physics by Bethe & Wilson [32] and Bethe in a sequence of papers [184], and interpreted as a global radial instability of the accretion envelope between the nascent neutron star and the stalled shock in the presence of sufficiently strong neutrino heating by Burrows & Goshy [34], is still considered as the standard paradigm for explaining how supernova explosions begin. But still a convincing demonstration of the viability of this mechanism and of its robustness in detailed numerical models has not been achieved. An exception may be progenitors stars in the 8–10 $M_\odot$ range, where new simulations with significantly improved and now very sophisticated neutrino transport have recently been able to confirm [58], at least qualitatively, the neutrino-driven explosions seen by Mayle & Wilson [60].

The undoubtedly greatest discovery in supernova theory after 1990 was the importance of hydrodynamic instabilities in the supernova core already during the very early moments of the explosion [63, 64, 65, 67]. While convection and mixing instabilities in supernovae and forming neutron stars were discussed earlier (e.g., [185, 186, 72, 36, 37]), the violence and the implications of convective instabilities in the neutrino-heated postshock layer had not been anticipated and was only recognized when the first two-dimensional and meanwhile even three-dimensional [70, 71] simulations became available. The presence of nonradial flow in the layer between gain radius and shock was found to significantly strengthen the neutrino-energy deposition there and to support the outward motion of the shock. It is now generally accepted to play a pivotal role for understanding the nature of the explosion mechanism, although the convectively supported neutrino-driven explosions obtained in the early multi-dimensional models with simple, grey neutrino diffusion [64, 65, 69] could not be reproduced by recent two-dimensional models with more elaborate, energy-dependent neutrino transport [11, 75]. In contrast, the increase of the neutrinospheric luminosities and mean neutrino energies by convection below the neutrinosphere, which had been suggested to be the key ingredient for robust explosions [185, 72, 187], has not been found to be of great relevance in state-of-the-art multi-dimensional models [12, 74, 75, 76].

More recently, theorists have recognized that not only convection takes place behind the stalled supernova shock, but that the accretion shock can be generically unstable to nonradial deformation [79, 83, 82, 81, 188]. This so-called SASI was found to lead to the preferred growth of low-mode deformation

and violent pulsational shock motion. The corresponding sloshing mode and anisotropic shock expansion does not only have the potential of giving support to the onset of neutrino-driven explosions more strongly than convection alone [12]. It was also claimed to instigate strong g-mode oscillations of the neutron star core that provide acoustic flux and thus power acoustically-driven explosions [75, 76]. In both cases the associated dipole and quadrupole asymmetries imprinted on the developing explosion have the potential to explain the origin of the observed high space velocities of pulsars [83, 84] and of the strong radial mixing and high nickel velocities observed to be present in Supernova 1987A [87]. A three-dimensional variant of the SASI may help giving neutron stars their natal spins [86].

A final breakthrough in our understanding of how supernova explosions work, generally accepted and based on self-consistent models with all relevant physics included, however, has not been achieved yet. Still even fundamental constraining parameters and ingredients are controversial. Do we understand the neutrino physics sufficiently well? Are our models correct in predicting the luminosities and mean energies of the radiated neutrinos? How important is rotation in the collapsing core? Do magnetohydrodynamic effects play a crucial role, tapping a large reservoir of free energy of rotation? Maybe the identification of such key aspects in the explosion mechanism will require observations that yield more direct evidence of what is going on in the supernova core than can be provided by explosion asymmetries, pulsar kicks or nucleosynthesis yields. The measurement of neutrino signals and gravitational waves will be able to yield such information, but that will require a galactic supernova to happen.

Meanwhile, waiting for such an event, theorists will continue to work on improved models, driven by the goal to advance their simulations to where the real world is, namely to the third dimension, and including the effects of general relativity in full beauty [189, 190]. Due to the decisive role played by neutrinos in the supernova core in governing the cooling and neutronization of the nascent neutron star, determining the thermodynamic conditions around the mass cut, and in setting the neutron-to-proton ratio in the supernova ejecta, an increasingly sophisticated incorporation of the neutrino physics and neutrino transport in future models is indispensable. In spherical symmetry, neutrino transport can now be treated by solving the multi-group Boltzmann transport problem [14, 8, 9]. This has led to the discovery that proton-rich conditions exist in the early neutrino-heated ejecta and thus p-processing can take place [169, 168, 11, 170, 179] as reviewed in this paper. In two-dimensional models "ray-by-ray-plus" transport can now handle the full energy-dependence of the problem with approximations to the non-radial transport [11, 12] or, alternatively, the transport in all spatial directions is described by making use of the diffusion approximation [98] but sacrificing the detailed treatment of the energy redistribution [76]. Ultimately, these shortcomings will have to be removed and modeling therefore faces the challenge of solving a five-dimensional, time-dependent transport problem in 2D and a 6-dimensional such problem in 3D [191].

Further improvements are also mandatory in the important microphysics that determines neutrino-matter interactions and the thermodynamic properties of the dense plasma in the stellar core. Weak magnetism corrections, nucleon recoil and thermal motions in neutrino-nucleon neutral-current and charged-current reactions (for a review of these effects, see [49]), as well as $\nu\bar{\nu}$ pair production in nucleon-nucleon bremsstrahlung and flavor-coupling neutrino-pair reactions turned out to have a noticeable impact on the emitted neutrino spectra, in particular leading to lower mean energies of the muon and tau neutrinos radiated during the supernova evolution [57, 56].

In their landmark paper Bethe, Brown, Applegate, and Lattimer [6] pointed out the dominance of electron captures on nuclei during the supernova collapse. In recent years the theoretical and numerical tools have become available to calculate the rates for the relevant weak-interaction processes at supernova conditions and, importantly, the theoretical model calculations could be constrained and guided by experimental data. As electron capture rates at supernova conditions are dominated by Gamow-Teller transitions, it has been particularly helpful that such transitions for several relevant nuclei could be measured by (n,p) and (d,^{2}He) charge-exchange experiments (e.g. [138, 134]), the latter reaction with impressive energy resolution. As shell model calculations reproduce these data — and the nuclear energy

spectra at low excitation energies — quite well, this many-body model has been applied to calculate the weak-interaction rates for nuclei that are abundant in the early phase of the collapse [120]. For heavier nuclei the rates have been obtained by another variant of the shell model (Shell Model Monte Carlo, [153]), which is capable of describing nuclear properties at non-zero temperatures considering the most important nucleon-nucleon correlations. These studies show that electron captures on nuclei are faster than on free protons during the infall stage, leading to significant quantitative modifications of stellar core collapse and core bounce, shock formation, and early shock propagation [153, 154, 42].

We have also briefly discussed the relevance of the equation of state for a variety of aspects in the supernova, ranging from the composition and deleptonization during collapse, the strength of the prompt shock, the compactness and temperatures and thus neutrino emission properties of the nascent neutron star, to the stagnation radius of the stalled shock. Both nuclear EoSs currently widely in use, the Lattimer & Swesty [117] and Shen et al. [116] EoSs, were derived on the basis of nuclear mean-field models. Comparisons between versions with soft and stiff phases, respectively, above $\sim 10^{14}\,\mathrm{g\,cm^{-3}}$, and with the Hartree-Fock EoS of Hillebrandt & Wolff [115] in 1D as well as 2D supernova simulations reveal sizable quantitative differences although such variations do not appear to be decisive for success or failure of the explosion. However, more work needs to be done along these lines, extending the simulations to later evolution stages and to a larger space of high-density EoS-possibilities.

Thus, improved microphysics has led to a more reliable description of supernova dynamics. Despite this progress, further improvements are desirable. Except for the famous $^{12}\mathrm{C}(\alpha,\gamma)^{16}\mathrm{O}$ rate, which, as Willy Fowler phrased it in his Nobel lecture [192], is of 'paramount importance' for the carbon-to-oxygen ratio in the Universe and for the evolution of stars, including their final fate as supernovae, there is probably no single nuclear datum which single-handedly influences the supernova dynamics. Rather it is an overwhelming wealth of nuclear input required for supernova simulations. This is not necessarily a disadvantage as it is impossible to directly measure nuclear rates under supernova conditions, mainly due to the non-zero temperature environment. Thus, individual nuclear rate uncertainties might average out in the supernova matter composition, provided such uncertainties are not systematic (like those discovered for the electron rates as discussed in some details in this review). Moreover, there is considerable hope that such systematic inaccuracies, if present, will be detected in the near future by a concerted effort of improved nuclear models and novel experimental tools and facilities. In fact, we are currently experiencing decisive advances in nuclear modelling with the development of many-body models, which, based on microscopic nuclear wave functions and realistic (or reasonable) nucleon-nucleon interactions, describe the low-energy nuclear spectra and properties. Furthermore, attempts are on the way to combine the progress in nuclear structure with the dynamics of reaction models. Certainly these models benefit from ever growing computational power, but they will decisively improve once the next generation of radioactive ion-beam facilities like RIBF at RIKEN and the Facility for Antiproton and Ion Research FAIR at GSI are operational. These facilities will allow the experimental determination of the properties of many of the unstable nuclei that are essential in many explosive astrophysical scenarios, including core-collapse supernovae. In particular, these facilities will advance our understanding of the isospin degree of freedom in nuclei and, more specifically for one of our major themes in this review, experiments with radioactive ion-beams will improve and constrain the nuclear models required to calculate the weak-interaction rates on nuclei during the core collapse by determining the single-particle structure and ground-state Gamow-Teller distributions for neutron-rich nuclei.

While radioactive ion-beam facilities will only indirectly contribute to the nuclear physics during the collapse, they will provide direct and essential nuclear data for supernova nucleosynthesis studies. Such crucial improvements range from precise mass measurements of heavy nuclei with $N \sim Z$, which will determine whether the νp process is indeed capable of producing the light p-nuclides [170, 179], to mass and halflive measurements for many r-process nuclei, hopefully removing the largest uncertainties in simulations of r-process nucleosynthesis. Certainly we see the break of dawn of a new and exciting era in nuclear astrophysics in general and in supernova modelling in particular.

Acknowledgements. Our research presented in this review has strongly benefitted from collaborations with R. Buras, E. Caurier, D.J. Dean, C. Fröhlich, A. Heger, W. Hillebrandt, W.R. Hix, R. Hoffman, A. Juodagalvis, M. Liebendörfer, O.E.B. Messer, A. Mezzacappa, E. Müller, P. von Neumann-Cosel, F. Nowacki, J. Pruet, M. Rampp, A. Richter, J.M. Sampaio, F.-K. Thielemann, and S.E. Woosley. The research in Garching was supported by Sonderforschungsbereich 375 on "Astro-Particle Physics" and Sonderforschungsbereich-Transregio 7 on "Gravitational Wave Astronomy" of the Deutsche Forschungsgemeinschaft. Computer time grants at the John von Neumann Institute for Computing (NIC) in Jülich, the Höchstleistungsrechenzentrum of the Stuttgart University (HLRS), the Leibniz-Rechenzentrum München, and the RZG in Garching are acknowledged.

References

[1] H.A. Bethe, Rev. Mod. Phys. **62** (1990) 801

[2] A. Mezzacappa, Ann. Rev. Nucl. Part. Sci **55** (2005) 467

[3] K. Kotake, K. Sato and K. Takahashi, Rept. Prog. Phys. **69** (2006) 971

[4] S. Woosley and H.-Th. Janka, Nature Physics **1** (2005) 147

[5] S. Woosley and J.S. Bloom, Ann. Rev. Astron. Astrophys. **44** (2006) 507

[6] H.A. Bethe, G.E. Brown, J. Applegate and J.M. Lattimer, Nucl. Phys. **A324** (1979) 487

[7] P.Goldreich and S.V. Weber, Ap.J. **238** (1980) 991

[8] T.A. Thompson, A. Burrows and P.A. Pinto, Ap.J. **592** (2003) 434

[9] M. Rampp and H.-Th. Janka, Ap.J. **539** (2000) L33

[10] R. Buras, M. Rampp, H.-Th. Janka and K. Kifonidis, Phys. Rev. Lett. **90** (2003) 241102

[11] R. Buras, M. Rampp, H.-Th. Janka and K. Kifonidis, Astron. Astrophys. **447** (2006) 1049

[12] R. Buras, Janka H.-Th., M. Rampp, and K. Kifonidis, Astron. Astrophys. **457** (2006) 281

[13] A. Mezzacappa *et al.*, Phys. Rev. Lett. **86** (2001) 1935

[14] M. Liebendörfer *et al.*, Phys. Rev. **D63** (2001) 103004

[15] M. Liebendörfer *et al.*, Nucl. Phys. **A719** (2003) 144c

[16] M. Liebendörfer *et al.*, Ap.J. Suppl. **150** (2004) 263

[17] M. Liebendörfer, M. Rampp, H.-Th. Janka and A. Mezzacappa, Ap.J. **620** (2005) 840

[18] H.-Th. Janka, R. Buras, F.S. Kitaura Joyanes, A. Marek and M. Rampp, in *Proc. 12th Workshop on Nuclear Astrophysics*, ed. by E. Müller and H.-Th. Janka, Report MPA/14 (MPI for Astrophysics, Garching, 2004) p. 150

[19] H.-Th. Janka, R. Buras, K. Kifonidis, A. Marek and M. Rampp, in *Cosmic Explosions*, ed. J.M. Marcaide and K.W. Weiler, (Springer, Berlin, 2005) p. 253 (astro-ph/0401461)

[20] H.-Th. Janka *et al.*, Nucl. Phys. **A758** (2005) 19c

[21] K. Sumiyoshi *et al.*, Ap.J. **629** (2005) 922

[22] J.R. Wilson, R. Mayle, S.E. Woosley and T. Weaver, Annals New York Acad. Sciences **470** (1986) 267

[23] E.S. Myra and S.A. Bludman, Ap.J. **340** (1989) 384

[24] S.W. Bruenn, in *Nuclear Physics in the Universe*, ed. by M.W. Guidry and M.R. Strayer, (Institute of Physics, Bristol, 1993) p. 31

[25] F.D. Swesty, J.M. Lattimer and E.S. Myra, Ap.J. **425** (1994) 195

[26] E. Baron and J. Cooperstein, Ap.J. **353** (1990) 597

[27] E. Baron, H.A. Bethe, G.E. Brown, J. Cooperstein and S. Kahana, Phys. Rev. Lett. **59** (1987) 736

[28] A. Burrows, Ann. Rev. Nucl. Sci. **40** (1990) 181

[29] A. Burrows and J.M. Lattimer, Ap.J. **307** (1986) 178

[30] A. Burrows, Ap.J. **334** (1988) 891

[31] J.R. Wilson, in *Numerical Astrophysics*, ed. by J.M. Centrella, J.M. LeBlanc and R.L. Bowers, (Jones and Bartlett, Boston, 1985) p. 422

[32] H.A. Bethe and J.R. Wilson, Ap.J. **295** (1985) 14

[33] S.A. Colgate, Nature **341** (1989) 489

[34] A. Burrows and J. Goshy, Ap.J. **416** (1993) L75

[35] H.-Th. Janka, Astron. Astrophys. **368** (2001) 527

[36] J.R. Wilson and R.W. Mayle, Phys. Reports **163** (1988) 63

[37] J.R. Wilson and R.W. Mayle, Phys. Reports **227** (1993) 97

[38] S.W. Bruenn and T. Dineva, Ap.J. **458** (1996) L71

[39] S.W. Bruenn, E.A. Raley and A. Mezzacappa, preprint (astro-ph/0404099)

[40] M. Liebendörfer, S. Rosswog and F.-K. Thielemann, Ap.J. Suppl. **141** (2002) 229

[41] M. Rampp and H.-Th. Janka, Astron. Astrophys. **396** (2002) 361

[42] A. Marek, H. Dimmelmeier, H.-Th. Janka, E. Müller and R. Buras, Astron. Astrophys. **445** (2006) 273

[43] S. W. Bruenn, Astrophys. J. Suppl. **58**, 771 (1985); A. Mezzacappa and S. W. Bruenn, Astrophys. J. **405**, 637 (1993); **410**, 740 (1993)

[44] C.J. Horowitz, Phys. Rev. **D55** (1997) 4577

[45] S.W. Bruenn and A. Mezzacappa, Phys. Rev. **D56** (1997) 7529

[46] N. Itoh, R. Asahara, N. Tomizawa, S. Wanajo and S. Nozawa, Ap.J. **611** (2004) 1041

[47] A. Marek, H.-Th. Janka, R. Buras, M. Liebendörfer and M. Rampp, Astron. Astrophys. **443** (2005) 201

[48] P.J. Schinder, Ap.J. Suppl. **74** (1990) 249

[49] C.J. Horowitz, Phys. Rev. **D65** (2002) 043001

[50] S. Reddy, M. Prakash and J.M. Lattimer, Phys.Rev. **D58** (1998) 013009

[51] S. Reddy, M. Prakash, J.M. Lattimer and J.A. Pons, Phys. Rev. **C59** (1999) 2888

[52] A. Burrows and R.F. Sawyer, Phys.Rev. **C58** (1998) 554

[53] A. Burrows and R.F. Sawyer, Phys.Rev. **C59** (1999) 510

[54] S. Hannestad and G. Raffelt, Ap.J. **507** (1998) 339

[55] T.A. Thompson, A. Burrows and J.E. Horvath, Phys. Rev. **C62** (2000) 035802

[56] R. Buras, H.-Th. Janka, M. Th. Keil, G. Raffelt and M. Rampp, Ap.J. **587** (2003) 320

[57] M. Th. Keil, G. Raffelt and H.-Th. Janka, Ap.J. **590** (2003) 971

[58] F.S. Kitaura, H.-Th. Janka and W. Hillebrandt, Astron. Astrophys. **450** (2006) 345

[59] K. Nomoto, Ap.J. **277** (1984) 791; Ap.J. **322** (1987) 206

[60] R. Mayle and J.R. Wilson, Ap.J. **334** (1988) 909

[61] K. Davidson and R.A. Fesen, Ann. Rev. Astron. Astrophys. **23** (1985) 119

[62] Nomoto K. *et al.*, Nature **299** (1982) 803

[63] M. Herant, W. Benz and S.A. Colgate, Ap.J. **395** (1992) 642

[64] M. Herant, W. Benz, W.R. Hix, C.L. Fryer and S.A. Colgate, Ap.J. **435** (1994) 339

[65] A. Burrows, J. Hayes and B.A. Fryxell, Ap.J. **450** (1995) 830

[66] H.-Th. Janka and E. Müller, Astron. Astrophys. **290** (1994) 496

[67] H.-Th. Janka and E. Müller, Astron. Astrophys. **306** (1996) 167

[68] A. Mezzacappa *et al.*, Ap.J. **495** (1998) 911

[69] C.L. Fryer, Ap.J. **522** (1999) 413

[70] C.L. Fryer and M.S. Warren, Ap.J. **574** (2002) L65

[71] C.L. Fryer and M.S. Warren, Ap.J. **601** (2004) 391

[72] A. Burrows, Ap.J. **318** (1987) L57

[73] W. Keil. H.-Th. Janka and E. Müller, Ap.J. **473** 1996) L111

[74] L. Dessart, A. Burrows, E. Livne and C.D. Ott, Ap.J. **645** (2006) 534

[75] A. Burrows, E. Livne, L. Dessart, C.D. Ott and J. Murphy, Ap.J. **640** (2006) 878

[76] A. Burrows, E. Livne, L. Dessart, C.D. Ott and J. Murphy, Ap.J., submitted (astro-ph/0610175)

[77] H.-Th. Janka, K. Kifonidis and M. Rampp, in *Physics of Neutron Star Interiors*, ed. by D. Blaschke, N.K. Glendenning and A. Sedrakian, (Springer, Berlin, 2001), p. 333 (astro-ph/0103015)

[78] T.A. Thompson, E. Quataert and A. Burrows, Ap.J. **620** (2005) 861

[79] J.M. Blondin, A. Mezzacappa and C. DeMarino, Ap.J. **584** (2003) 971

[80] T. Foglizzo, Astron. Astrophys. **368** (2001) 311; **392** (2002) 353

[81] T. Foglizzo, P. Galletti, L. Scheck and H.-Th. Janka, Ap.J., in press (astro-ph/0606640)

[82] J.M. Blondin and A. Mezzacappa, Ap.J. **642** 401

[83] L. Scheck, T. Plewa, H.-Th. Janka, K. Kifonidis and E. Müller, Phys. Rev. Lett. **92** 011103

[84] L. Scheck, K. Kifonidis H.-Th. Janka and E. Müller, Astron. Astrophys. **457** (2006) 963

[85] H.-Th. Janka, L. Scheck, K. Kifonidis, E. Müller and T. Plewa, in *The Fate of the Most Massive Stars*, ed. by R. Humphreys and K. Stanek, (Astronomical Society of the Pacific, San Francisco, 2005), p. 363 (astro-ph/0408439)

[86] J.M. Blondin and A. Mezzacappa, Nature, in press (astro-ph/0611680)

[87] K. Kifonidis, T. Plewa, L. Scheck, H.-Th. Janka and E. Müller E., Astron. Astrophys. **453** (2006) 661

[88] A. Socrates, O. Blaes, A. Hungerford and C.L. Fryer, Ap.J. **632** (2005) 531

[89] J.R. Wilson, G.J. Mathews and H.E. Dalhed, Ap.J. **628** (2005) 335

[90] J.C. Wheeler, D.L. Meier and J.R. Wilson, Ap.J. **568** (2002) 807

[91] S. Akiyama, J.C. Wheeler, D.L. Meier and I. Lichtenstadt, Ap.J. **584** (2003) 954

[92] S. Yamada and H. Sawai, Ap.J. **608** (2004) 907

[93] N.V. Ardeljan, G.S. Bisnovatyi-Kogan and S.G. Moiseenko, Mon. Not. R. Astron. Soc. **359** (2005) 333

[94] M. Obergaulinger, M.A. Aloy and E. Müller, Astron. Astrophys. **450** (2006) 1107

[95] A. Heger, S.E. Woosley and H.C. Spruit, Ap.J. **626** (2005) 350

[96] C.Y. Cardall, E.J. Lentz and A. Mezzacappa, Phys. Rev. **D72** (2005) 043007; C.Y. Cardall, Nucl. Phys. B (Proc. Suppl.) **145** (2005) 295; C.Y. Cardall and A. Mezzacappa, Phys. Rev. **D68** (2003) 023006; arXiv-paper astro-ph/0404401

[97] E. Livne, A. Burrows, R. Walder, I. Lichtenstadt and T.A. Thompson, Ap.J. **609** (2004) 277

[98] F.D. Swesty and E.S. Myra, Ap.J., submitted (astro-ph/0607281)

[99] I. Hubeny and A. Burrows, Ap.J., submitted (astro-ph/0609049)

[100] H. Duan, G.M. Fuller, J. Carlson and Y.-Z. Qian, Phys. Rev. **D74** (2006) 105014; arXiv-preprint astro-ph/0608050

[101] S. Hannestad, G.G. Raffelt, G. Sigl and Y.Y.Y. Wong, Phys. Rev. **D74** (2006) 105010

[102] G. Baym, H.A. Bethe and C.J. Pethick, Nucl. Phys. **A175** (1971) 225

[103] S.E. Woosley and T.A. Weaver, Ap.J. Suppl. **101** (1995) 181

[104] A. Heger, S.E. Woosley, G. Martínez-Pinedo and K. Langanke, Ap.J. **560** (2001) 307

[105] W.R. Hix and F.-K. Thielemann, ApJ **460** (1996) 869

[106] W.R. Hix, Ph.D. thesis, Harvard University (1995)

[107] E. Bravo and D. García-Senz, Mon. Not. Roy. Ast. Soc. **307**, 984 (1999)

[108] D.G. Ravenhall, C.J. Pethick and J.R. Wilson, Phys. Rev. Lett. **50** (1983) 2066

[109] R.D. Williams and S.E. Koonin, Nucl. Phys. **A435** (1985) 844

[110] G. Watanabe, K. Sato, K. Yasuoka and T. Ebisuzaki, Phys. Rev. **C69** (2004) 055805

[111] P. Magierski and A. Bulgac, Acta Phys. Polon. **B35** (2004) 1203

[112] E. Khan, N. Sandalescu and N. van Giai, Phys. Rev. **C71** (2005) 042801

[113] C.J. Horowitz, M.A. Perez-Garcia, D.K. Berry and J. Piekarewicz, Phys. Rev. **C72** (2005) 035801

[114] A. Burrows and J.M. Lattimer, Ap. J. **307** (1986) 178

[115] W. Hillebrandt, R.G. Wolff and K. Nomoto, Astron. Astrophys. **133** (1984) 175; W. Hillebrandt and R.G. Wolff, in *Nucleosynthesis: Challenges and New Developments*, ed. by W.D. Arnett and J.W. Truran, (Univ. Chicago Press, Chicago, 1985), p. 131; W. Hillebrandt, in *Supernovae*, ed. by S.A. Bludman, R. Mochkovitch and J. Zinn-Justin, (North-Holland, Amsterdam, 1994), p. 251

[116] H. Shen, H. Toki, K. Oyamatsu and K. Sumiyoshi, Nucl. Phys. **A637** (1998) 435; Prog. Theor. Phys. **100** (1998) 1013

[117] J.M. Lattimer and F.D. Swesty, Nucl. Phys. **A535** (1991) 331; J.M. Lattimer, C.J. Pethick, D.G. Ravenhall and D.Q. Lamb, Nucl. Phys. **A432** (1985) 646

[118] F. Weber, Prog. Part. Nucl. Phys. **54** (2004) 193

[119] G.M. Fuller, W.A. Fowler and M.J. Newman, ApJS **48** (1982) 279

[120] K. Langanke and G. Martínez-Pinedo, Nucl. Phys. **A673** (2000) 481

[121] A. Marek, Diploma Thesis, Technische Universität München (2003)

[122] A. Marek, PhD Thesis, Technische Universität München (2006)

[123] I.S. Towner and J.C. Hardy, in *Symmetries and Fundamental Interactions in Nuclei*, eds. W.C. Haxton and E.M. Henley (World Scientific, Singapore, 1995) p.183.

[124] A. R. Edmons, *Angular momentum in Quantum Mechanics* (Princeton University Press, Princeton, New Jersey, 1960)

[125] F. Osterfeld, Rev. Mod. Phys. **64** (1992) 491.

[126] G. Martínez-Pinedo, A. Poves, E. Caurier, and A. P. Zuker, Phys. Rev. C **53** (1996) R2602.

[127] K.I. Ikeda, S. Fujii and J.I. Fujita, Phys. Lett. **3** (1963) 271

[128] C. Gaarde, Nucl. Phys. **A396** (1983) 127c

[129] A.L. Williams *et al.*, Phys. Rev. **C51** (1995) 1144

[130] B. A. Brown and B H. Wildenthal, At. Data Nucl. Data Tables **33** (1985) 347.

[131] K. Langanke, D. J. Dean, P. B. Radha, Y. Alhassid, and S. E. Koonin, Phys. Rev. C **52** (1995) 718.

[132] H. Sakai, Nucl. Phys. **A690** (2001) 66c

[133] Y. Fujita *et al.*, EPJA **13** (2002) 411

[134] D. Frekers, Prog. Part. Nucl. Phys. **57** (2006) 217

[135] G.M. Fuller, W.A. Fowler and M.J. Newman, ApJS **42** (1980) 447

[136] G.M. Fuller, W.A. Fowler and M.J. Newman, ApJ **252** (1982) 715

[137] G.M. Fuller, W.A. Fowler and M.J. Newman, ApJ **293** (1985) 1

[138] W.P. Alford *et al.*, Phys. Rev. **C48** (1993) 2818

[139] T. Rönnquist *et al.*, Nucl. Phys. **A563** (1993) 225

[140] S. El-Kateb *et al.*, Phys. Rev. **C49** (1994) 3128

[141] E. Caurier, K. Langanke, G. Martínez-Pinedo and F. Nowacki, Nucl. Phys. A **653** (1999) 439.

[142] C. Bäumer *et al.*, Phys. Rev. **C68** (2003) 031303(R)

[143] G. Martínez-Pinedo, K. Langanke and D.J. Dean, Ap.J. Suppl. **126** (2000) 493

[144] M.B. Aufderheide, I. Fushiki, G.M. Fuller and T.A. Weaver, Ap.J. **424** (1994) 389

[145] D. Frekers, private communication

[146] K. Langanke, E. Kolbe and D.J. Dean, Phys. Rev. **C63** (2001) 032801

[147] S.E. Koonin, D.J. Dean and K. Langanke, Phys. Rep. **278** (1997) 2

[148] P.B. Radha, D.J. Dean, S.E. Koonin, K. Langanke and P. Vogel, Phys. Rev. **C56** (1997) 3097

[149] A. Heger, K. Langanke, G. Martínez-Pinedo and S.E. Woosley, Phys. Rev. Lett. **86** (2001) 1678

[150] G.M. Fuller, Ap.J. **252** (1982) 741

[151] J.M. Sampaio, doctoral thesis, Aarhus University (2003)

[152] J. Cooperstein and J. Wambach, Nucl. Phys. **A420** (1984) 591

[153] K. Langanke *et al.*, Phys. Rev. Lett. 90 (2003) 241102

[154] R.W. Hix *et al.*, Phys. Rev. Lett. **91** (2003) 210102

[155] A. Marek *et al.*, in preparation

[156] W.C. Haxton, Phys. Rev. Lett. **60** (1988) 1999

[157] S.W. Bruenn and W.C. Haxton, Ap.J. **376** (1991) 678

[158] J.M. Sampaio, K. Langanke and G. Martínez-Pinedo, Phys. Lett. **B511** (2001) 11

[159] J.M. Sampaio, K. Langanke, G. Martínez-Pinedo and D.J. Dean, Phys. Lett. **B529** (2002) 19

[160] K. Langanke, G. Martínez-Pinedo, P. v. Neumann-Cosel and A. Richter, Phys. Rev. Lett. **93** (2004) 202501

[161] P. v. Neumann-Cosel *et al.*, Phys. Lett. **B443** (1998) 1

[162] A. Juodagalvis *et al.*, Nucl. Phys. **A747** (2005) 87

[163] B. Müller, H.-Th. Janka, K. Langanke *et al.*, to be published

[164] S.E. Woosley, A. Heger and T.A. Weaver, Rev. Mod. Phys. **74** (2002) 1015

[165] M. Hashimoto, Prog. Theor. Phys. **94** (1995) 663

[166] H.-Th. Janka, R. Buras and M. Rampp, Nucl. Phys. **A718** (2003) 269

[167] M. Liebendörfer, A. Mezzacappa, F.-K. Thielemann, O.E. Bronson Messer, W.R. Hix and S.W. Bruenn, Phys. Rev. D63 (2001) 103004

[168] C. Fröhlich *et al.*, Nucl. Phys. **A758** (2004) 28c

[169] J. Pruet, S.E. Woosley, R. Buras, H.-Th. Janka and R.D. Hoffman, ApJ **623** (2005) 325

[170] C. Fröhlich, G. Martínez-Pinedo *et al.*, ApJ **637** (2006) 415

[171] H. Schatz *et al.*, Phys. Rep. **294** (1998) 167

[172] C. Fröhlich, G. Martínez-Pinedo *et al.*, Phys. Rev. Lett. **96** (2006) 142505

[173] S. Wanajo, ApJ **647** (2006) 1323

[174] Y-Z. Qian and G.M. Fuller, Phys. Rev. **D52** (1995) 656

[175] Y.-Z. Qian and S.E. Woosley, ApJ **471** (1996) 331

[176] S.E. Woosley, J.R. Wilson, G.J. Mathews, R.D. Hoffman and B.S. Meyer, Ap.J. **433** (1994) 229

[177] K. Takahashi, J. Witti and H.-Th. Janka, Astron. Astrophys. **286** (1994) 857

[178] S. Wanajo, T. Kajino, G.J. Mathews and K. Otsuki, Ap.J. **554** (2001) 578

[179] J. Pruet, R.D. Hoffman, S.E. Woosley, H.-Th. Janka and R. Buras, ApJ **644** (2006) 1028

[180] A. Frebel *et al.*, Nature **434** (2005) 871

[181] S.E. Woosley, Ap.J. **405** 273

[182] A.I. MacFadyen and S.E. Woosley, Ap.J. **524** (1999) 262

[183] S.A. Colgate and R.H. White, Ap.J. **143** (1966) 626

[184] H.A. Bethe, Ap.J. **412** (1993) 192; **449** (1995) 714; **469** (1996) 737; **473** (1996) 343; **490** (1997) 765; Nucl. Phys. **A606** (1996) 95

[185] H.A. Bethe, G.E. Brown and J. Cooperstein, Ap.J. **322** (1987) 201

[186] A. Burrows and J.M. Lattimer, Phys. Rep. **163** (1988) 51

[187] A. Burrows and B.A. Fryxell, Science **258** (1992) 430

[188] N. Ohnishi, K. Kotake and S. Yamada, Ap.J. **641** (2006) 1018

[189] M. Shibata and Y.-I. Sekiguchi, Phys. Rev. **D71** (2005) 024014

[190] C.D. Ott *et al.*, Phys. Rev. Lett., submitted (astro-ph/0609819)

[191] C.Y. Cardall, A.O. Razoumov, E. Endeve and A. Mezzacappa, in *Open Issues in Understanding Core Collapse Supernovae*, World Scientific, in press (astro-ph/0510704)

[192] W.A. Fowler, Rev. Mod. Phys. **56** (1984) 149